International Journal of
Molecular Sciences

MDPI

Article

Soluble Prion Peptide 107–120 Protects Neuroblastoma SH-SY5Y Cells against Oligomers Associated with Alzheimer's Disease

Elham Rezvani Boroujeni [1,2], Seyed Masoud Hosseini [1,*], Giulia Fani [2], Cristina Cecchi [2] and Fabrizio Chiti [2,*]

1 Department of Microbiology and Microbial Biotechnology, Faculty of Life Science and Biotechnology, Shahid Beheshti University, Tehran 1983969411, Iran; e_rezvaniboroujeni@sbu.ac.ir
2 Department of Experimental and Clinical Biomedical Sciences, University of Florence, Viale G.B Morgagni 50, 50134 Florence, Italy; giulia.fani@unifi.it (G.F.); cristina.cecchi@unifi.it (C.C.)
* Correspondence: Ma_Hosseini@SBU.AC.IR (S.M.H.); fabrizio.chiti@unifi.it (F.C.); Tel.: +98-21-29905913 (S.M.H.); +39-0552751220 (F.C.)

Received: 6 August 2020; Accepted: 28 September 2020; Published: 1 October 2020

Abstract: Alzheimer's disease (AD) is the most prevalent form of dementia and soluble amyloid β (Aβ) oligomers are thought to play a critical role in AD pathogenesis. Cellular prion protein (PrP^C) is a high-affinity receptor for Aβ oligomers and mediates some of their toxic effects. The *N*-terminal region of PrP^C can interact with Aβ, particularly the region encompassing residues 95–110. In this study, we identified a soluble and unstructured prion-derived peptide ($PrP_{107–120}$) that is external to this region of the sequence and was found to successfully reduce the mitochondrial impairment, intracellular ROS generation and cytosolic Ca^{2+} uptake induced by oligomeric $Aβ_{42}$ ADDLs in neuroblastoma SH-SY5Y cells. $PrP_{107–120}$ was also found to rescue SH-SY5Y cells from $Aβ_{42}$ ADDL internalization. The peptide did not change the structure and aggregation pathway of $Aβ_{42}$ ADDLs, did not show co-localization with $Aβ_{42}$ ADDLs in the cells and showed a partial colocalization with the endogenous cellular PrP^C. As a sequence region that is not involved in Aβ binding but in PrP self-recognition, the peptide was suggested to protect against the toxicity of $Aβ_{42}$ oligomers by interfering with cellular PrP^C and/or activating a signaling that protected the cells. These results strongly suggest that $PrP_{107–120}$ has therapeutic potential for AD.

Keywords: Alzheimer's disease; prion peptide; Aβ oligomers; ADDLs

1. Introduction

Alzheimer's Disease International (ADI) and the American Alzheimer's Association (AA) have estimated that over than 50 million people are living with dementia, and that Alzheimer's disease (AD) is the most common cause and may account for 60–70% of dementia cases [1]. According to this, these numbers will increase dramatically, and this disease will considerably challenge the world healthcare system in the future.

Evidence indicates that AD is an aging-related disease, and frequency in individuals aged 85 or older is higher (one in three) compared to age 65 (one in nine) [1,2]. AD involves a loss of memory, cognitive impairment and behavioral instability [3]. Both extracellular neuritic plaques mainly composed of the amyloid beta (Aβ) peptide and intraneuronal neurofibrillary tangles containing the hyperphosphorylated tau protein are important histopathological hallmarks associated with AD [4,5].

Although accumulation of senile plaques formed by Aβ is a major histopathological trait of AD, it is widely accepted that soluble Aβ oligomers, forming as intermediate species in the process of neuritic plaque formation or released from the plaques, can effectively play a key role in neuronal

dysfunction and impair synaptic structure and function [6,7]. It is well-known that such oligomers can inhibit long-term potentiation (LTP)—a correlate of synaptic plasticity [8,9]—as well as activating expression of the complement system [10,11] and general neurotoxic [6,12].

Several studies have reported that the cell membrane protein PrP^C mediates the abnormal effects of Aβ oligomers, particularly the oligomer-induced inhibition of LTP [13–15]. It was also reported that memory deficits in AD transgenic mice require the presence of PrP^C [16], and that loss of synaptic markers, axonal degeneration and early death in transgenic mice are fully dependent on PrP^C [17]. Other reports have shown that co-expression of PrP^C and Aβ reduces longevity in *Drosophila melanogaster*, and that expression of Aβ individually cannot create pathogenic phenotypes [18]. In spite of the large body of evidence that PrP^C mediates the aberrant effects of Aβ oligomers, other studies have indicated that it is not a necessary component for the toxicity cascade induced by Aβ oligomers, as Aβ-induced LTP inhibition or memory impairment has also been reported to occur independently of the overexpression or ablation of PrP^C in the transgenic mice [19–21]. This has led to a controversy that remains unresolved [22].

PrP^C is a membrane protein that is found in both neurons and glial cells [23] and has been proposed to have a role in cellular signaling, copper homeostasis, cell adhesion and even neuroprotection [24,25]. The mature form of human PrP^C consists of a single polypeptide chain of 208 amino acid residues (residues 23–230). The *N*-terminal region of the protein (residue 23–120) is unstructured, while the *C*-terminal region (residues 121–230) is largely structured, consisting of three α-helices (residues 144–154, 173–194, 200–228) and two short anti-parallel β-strands (residues 128–131, 161–164) [26]. The protein is anchored to the cell membrane via a glycosyl-phosphatidyl-inositol (GPI) anchor encompassing residues 231–253, which is excised in the mature form [26–28]. PrP^C function is poorly understood, although roles have been suggested in synaptic transmission, long-term memory, circadian rhythms, T cell function, hematopoietic stem cell renewal, copper-binding, apoptosis and oxidative stress homeostasis, among others [29]. The scrapie form (PrP^{Sc}) is derived from PrP^C [30–32]. The central event is the conversion from an α-helix rich structure to a form with a high β-sheet content. Accumulation of this infectious misfolded form of prion protein (PrP^{Sc}) can cause a group of neurodegenerative diseases affecting both human and animals [30–32].

A large number of data have shown that PrP^C has a high binding affinity for $A\beta_{42}$ oligomers [33,34]. Even studies showing that PrP^C-expressing and PrP^C knock-out mice were equally susceptible to $A\beta_{42}$ oligomer-induced cognitive impairment recognized that the oligomers interacted with PrP^C with high affinity [19]. The first evidence of binding between $A\beta_{42}$ oligomers and PrP^C dates back to 2009, when it was also found that the *N*-terminal region of PrP^C, particularly the 95–110 residues, was involved in the binding [35]. One year later, Chen and co-workers showed that both *N*-terminal residues 23–27 and 92–110 were critically important for binding [36]. The importance of these two sequence regions was then confirmed by later reports [13,14,37–42].

Unlike the many reports showing a role of the *N*-terminal region of PrP^C in the binding of Aβ oligomers, none of the studies reported so far have highlighted a role of the region encompassing residues 106–126 in $A\beta_{42}$ oligomer binding [34]. By contrast, this PrP segment was found to be mainly responsible for prion aggregation [43–49]. The AGAAAAGA palindromic sequence 113–120, in particular, is necessary for PrP^C-PrP^{Sc} interaction [44,45], and the two glycine residues at positions 114 and 119 have been suggested as particularly important for fibril formation [50].

As a segment involved in PrP self-recognition, but not in Aβ-PrP^C complex formation, we reasoned that a short peptide encompassing this region of the sequence might inhibit $A\beta_{42}$ oligomer toxicity. The hypothesis for this idea is that such a peptide might leave the Aβ oligomers unbound and unaltered, while engaging in interactions with PrP^C. Our designed peptide encompassing residues 107–120 ($PrP_{107–120}$) was found to be very soluble in physiological conditions, most probably because it lacks the highly hydrophobic region VVGGLG (residues 121–126) of the PrP^C fragment 106–126 responsible for prion aggregation [44,45,49]. Importantly, the peptide was found to prevent the generic toxic effects of $A\beta_{42}$ oligomers on neuroblastoma SH-SY5Y cells in absence of $A\beta_{42}$ oligomer binding

and structural reorganization, but in presence of partial binding between $PrP_{107–120}$ peptide and endogenous cellular PrP^C. Since this peptide is not aggregation-prone and has beneficial effects against Aβ-induced toxicity, it is of potentially great interest for rationalizing the pathogenesis of AD and routes to its prevention, as well as in setting up therapeutic strategies for the treatment of AD.

2. Results

2.1. Freshly Dissolved $PrP_{107–120}$ is Monomeric

We calculated the theoretical hydrodynamic radius (R_h) for a peptide with the size of $PrP_{107–120}$ (14 amino acid residues) in an unfolded state, using the equation described in Section 4, and previously published in [51]. According to this equation, the R_h value was found to be 0.99 ± 0.56 nm. Dynamic light scattering (DLS) shows that $PrP_{107–120}$ dissolved in water has a hydrodynamic diameter (D_h) of 2.11 ± 0.68 nm, corresponding to a R_h of 1.05 ± 0.34 nm (Figure 1), which is in good agreement with that estimated theoretically. The DLS distribution also showed very large $PrP_{107–120}$ aggregates at 70–7000 nm, but these are quantitatively irrelevant, as light scattering intensity is known to scale with the sixth power of the size. These results reveal that $PrP_{107–120}$ dissolved in water is unfolded and predominantly non-aggregated.

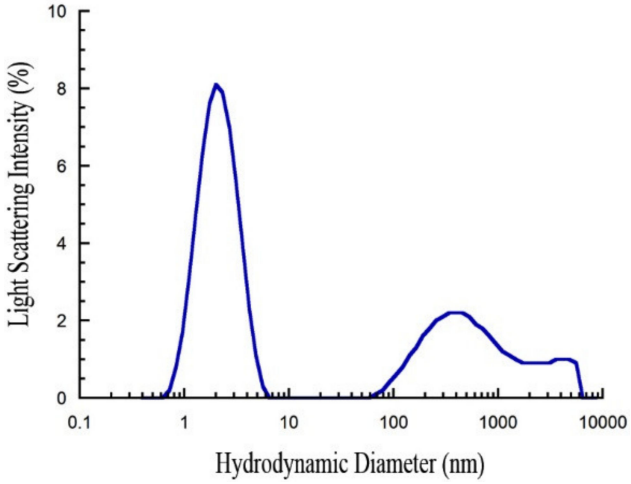

Figure 1. Size distribution of $PrP_{107–120}$. Size distribution by light scattering intensity obtained with dynamic light scattering (DLS) for $PrP_{107–120}$ dissolved in plain water at 25 °C. Peptide concentration was 1 mg/mL. The large aggregates at 70–7000 nm are quantitatively irrelevant, as light scattering intensity scales with the sixth power of the size.

2.2. $PrP_{107–120}$ Remains Monomeric and Unstructured under Different Conditions

We then investigated whether different conditions that are generally favorable for protein aggregation have the ability to promote fibrillation for the designed peptide. The different conditions are listed in Section 4 and include various peptide concentrations, salt concentrations, pH values and co-solvents. As a representative example, we show the results obtained at 1.0 mg/mL peptide in 20 mM phosphate buffer, 200 mM Na_2SO_4, with a pH 7.0, at 37 °C (Figure 2). The DLS distribution showed a D_h of ~1 nm immediately after incubation (0 h) under these conditions, which appears dominant in the population if we take into account that the intensity of scattered light scales with the sixth power of the diameter (Figure 2A). This peak is still clearly visible even after 5 days incubation under these conditions (Figure 2A). Aggregates increased in population after 5 days, yet they appear to be quantitatively irrelevant if we consider the relationship between scattered light intensity and diameter mentioned above. The Thioflavin T (ThT) fluorescence did not increase following the addition of the peptide after 5 days incubation under these conditions relative to the blank containing only ThT (Figure 2B), and the far-UV circular dichroism (CD) spectrum also remained unchanged with a single

negative peak at ~198 nm, which is typical of highly disordered states (Figure 2C). Hence, we did not observe a ThT-positive structure or significant changes in size and CD spectrum even after 5 days incubation. Similar results were obtained in all conditions tested (data not shown), indicating that $PrP_{107–120}$ is soluble and stable under all the conditions studied here that are, by contrast, potentially favorable for amyloid fibril formation.

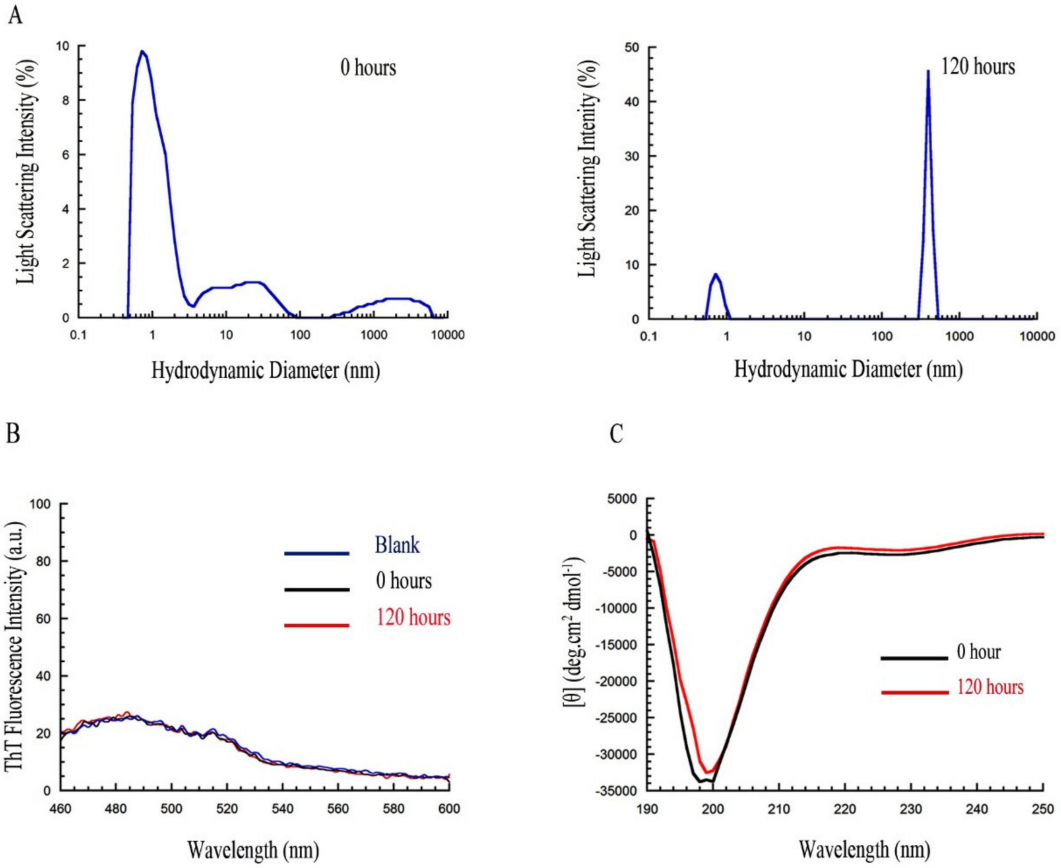

Figure 2. Effect of 20 mM phosphate buffer, 200 mM Na_2SO_4, pH 7.0, 37 °C on $PrP_{107–120}$ (1.0 mg/mL) aggregation. (**A**) Size distributions by light scattering intensity of the peptide sample obtained with DLS at t = 0 h (left) and 120 h (right) under the conditions described above. (**B**) Thioflavin T (ThT) fluorescence spectra with buffer (blank) and $PrP_{107–120}$ sample after 0 and 120 h. Peptide sample was incubated as described above. ThT assay was carried out at 22 µM ThT, 0.12 mg/mL $PrP_{107–120}$ (final concentrations in the cuvette), pH 6.0, 37 °C. (**C**) Far-UV circular dichroism (CD) spectra of $PrP_{107–120}$ incubated for 0 and 120 h. Peptide sample was incubated as described above and diluted to 0.2 mg/mL in the same buffer before spectrum acquisition at 25 °C.

2.3. *$PrP_{107-120}$ Reduces $A\beta_{42}$ Cytotoxicity on SH-SY5Y Cells*

In order to analyze whether $PrP_{107-120}$ can rescue the cellular dysfunction induced by $A\beta_{42}$ oligomers, we used amyloid-derived diffusible ligands (ADDLs) formed from $A\beta_{42}$ peptide according to a well-established protocol [52]. ADDLs were chosen as representative $A\beta_{42}$ oligomers because they are widely used [52–55], and their morphology and purity are routinely verified [56,57]. These have been found to be toxic and increase intracellular Ca^{2+} and reactive oxygen species (ROS) levels in cultured cells [53,58], and have been found in post-mortem AD brains using both polyclonal and monoclonal conformation-sensitive antibodies specific to ADDLs [54,59]. To this aim, we analyzed the effects of $A\beta_{42}$ ADDLs with a final concentration of 3-µM monomer equivalents (m.e.) on the metabolic activities of human SH-SY5Y cells. This immortalized neuronal cell model is mostly used for

AD research, as human cholinergic neurons are difficult to obtain and maintain and unsuitable for routine experiments.

The metabolic activity of the cells was analyzed using the 3-(4,5-dimethylthiazol-2-yl)-2,5-diphenyltetrazolium bromide (MTT) assay, which is a widely used indicator of mitochondrial reduction capacity. The ability of SH-SY5Y cells to reduce MTT significantly decreased to 66.6 ± 4.5% following treatment for 24 h with $A\beta_{42}$ ADDLs at 3 μM m.e. (Figure 3). By contrast, no detectable change was observed in cells treated with $PrP_{107–120}$ and monomeric $A\beta_{42}$ at final concentrations of 0.75 and 3 μM, respectively (Figure 3). The addition of the $PrP_{107–120}$ (0.75 μM) to $A\beta_{42}$ ADDLs (3 μM) significantly increased cell viability to 79.7 ± 4.3% compared with the cells treated with $A\beta_{42}$ ADDLs (3 μM) in the absence of the peptide (Figure 3). In another experiment, $PrP_{107–120}$ at a concentration of 0.75 μM was added to monomeric $A\beta_{42}$ peptide at a concentration of 3 μM, and the resulting sample was maintained under conditions favorable for ADDL formation before addition to the cells ($A\beta_{42}$ + $PrP_{107–120}$). In this case, we found a cell viability of 86.4 ± 2.5%, again indicating protection by the $PrP_{107–120}$ peptide. These results suggest that $PrP_{107–120}$ can act as an inhibitor of $A\beta_{42}$ ADDL oligomer toxicity.

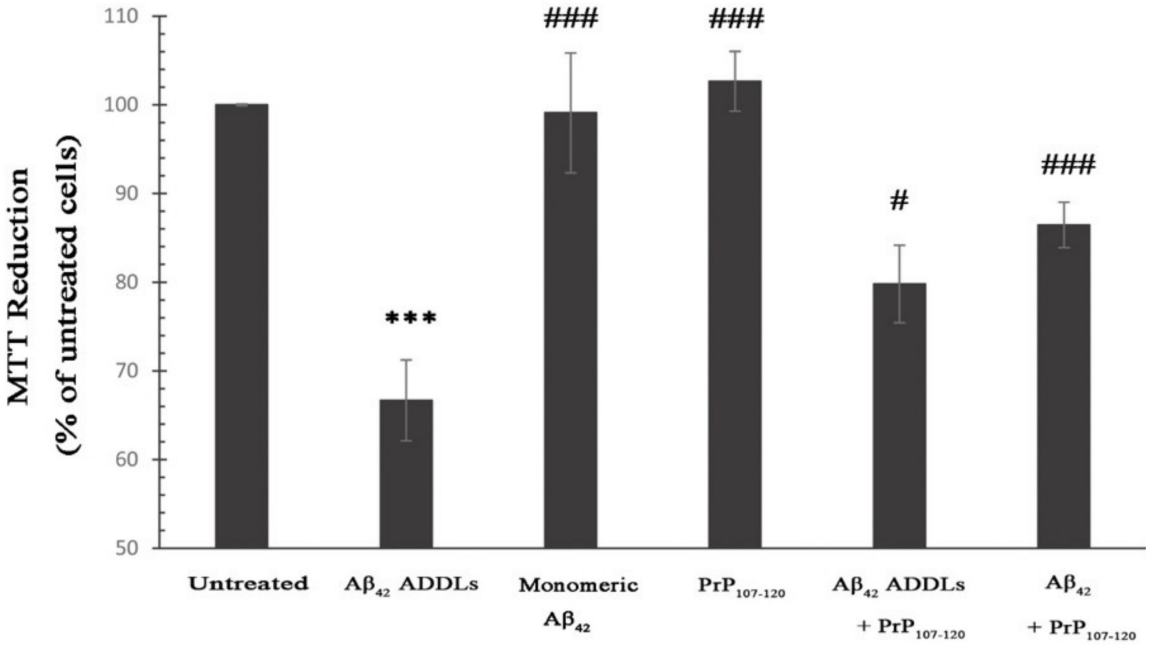

Figure 3. Cell viability assay in the presence of $A\beta_{42}$ oligomers and $PrP_{107–120}$. 3-(4,5-dimethylthiazol-2-yl)-2,5-diphenyltetrazolium bromide (MTT) reduction capacity of SH-SY5Y cells following 24 h treatment with $A\beta_{42}$ amyloid-derived diffusible ligands (ADDLs), monomeric $A\beta_{42}$, $PrP_{107–120}$, $A\beta_{42}$ ADDLs + $PrP_{107–120}$ and $A\beta_{42}$ and $PrP_{107–120}$ pre-incubated under conditions promoting ADDL formation prior to addition to the cell medium. All samples were initially in 2% (*v*/*v*) dimethyl sulfoxide (DMSO) and F-12 Ham medium at concentrations of 100 and 25 μM (m.e.) for $A\beta_{42}$ and $PrP_{107–120}$, respectively, and were diluted 33-fold before each experiment into cellular medium without DMSO to final concentrations of 3 and 0.75 μM (m.e.) for $A\beta_{42}$ and $PrP_{107–120}$, respectively. The data shown are mean values ± SEM of five independent experiments. The triple asterisks (***) refer to p values < 0.001 relative to the untreated cells. The single (#) and triple (###) symbols refer to p values < 0.05 and < 0.001, respectively, relative to $A\beta_{42}$ ADDLs.

2.4. $PrP_{107-120}$ Reduces Ca^{2+} Influx Induced by $A\beta_{42}$ Oligomers

An early cellular insult caused by $A\beta_{42}$ ADDLs, and $A\beta_{42}$ oligomers more generally, when added to the cellular medium, is the permeabilization of the plasma membrane with a rapid influx of calcium ions (Ca^{2+}) from the extracellular space to the cytosol [53,58,60]. To investigate whether $PrP_{107–120}$ can prevent the increase of Ca^{2+} levels mediated by the $A\beta_{42}$ ADDL oligomers, we monitored the influx of Ca^{2+} in SH-SY5Y cells treated with $A\beta_{42}$ ADDLs in presence and absence of $PrP_{107–120}$, at the

same concentrations used for the MTT assay. The quantification of the intracellular Ca^{2+}-derived fluorescence in confocal microscopy images shows that the treatment of the cells with $A\beta_{42}$ ADDLs caused a significant increase in intracellular Ca^{2+} up to 246 ± 21% compared with untreated cells, taken as 100% (Figure 4). By contrast, the cellular exposure to $A\beta_{42}$ + $PrP_{107–120}$, $A\beta_{42}$ ADDLs + $PrP_{107–120}$ and $PrP_{107–120}$ alone triggered a minor increase of intracellular Ca^{2+}-derived fluorescence (i.e., to 116 ± 13%, 132 ± 7% and 130 ± 11% respectively) that was significantly lower than that observed in cells treated with $A\beta_{42}$ ADDLs (Figure 4). This result suggests a protective role of $PrP_{107–120}$ in the Ca^{2+} influx mediated by the $A\beta_{42}$ oligomers in neuronal cells. Since the concentrations of Ca^{2+} and $PrP_{107–120}$ in the cell medium were 2 mM and 0.75 μM, respectively, it can be ruled out that the inhibition of ADDL-induced Ca^{2+} influx mediated by the prion peptide arises from peptide-Ca^{2+} binding, as the peptide is over three orders of magnitude sub-stoichiometric.

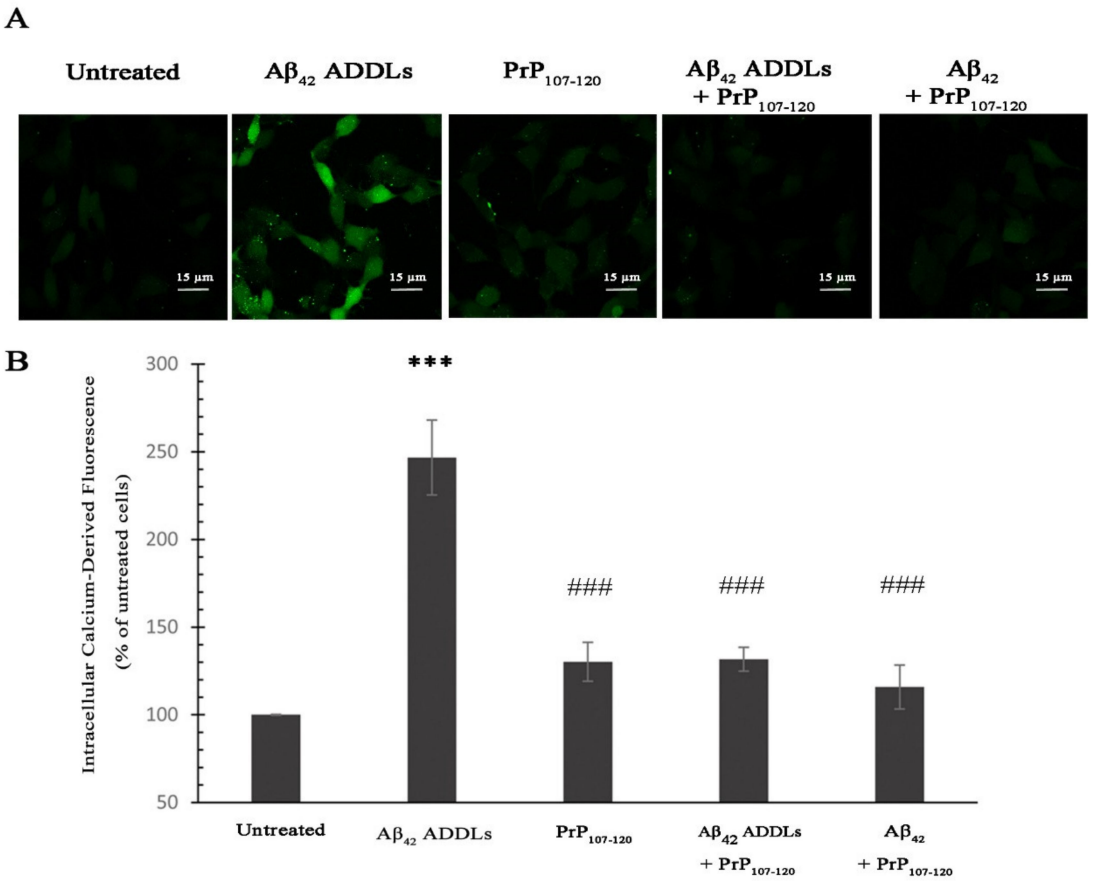

Figure 4. Analysis of intracellular Ca^{2+} levels of SH-SY5Y cells treated with $A\beta_{42}$ oligomers and $PrP_{107–120}$. (**A**) Representative scanning confocal microscopy images of intracellular free Ca^{2+} levels in SH-SY5Y cells loaded with Fluo-4 AM probe. The cells were treated for 1 h with $A\beta_{42}$ ADDLs, $PrP_{107–120}$, $A\beta_{42}$ ADDLs + $PrP_{107–120}$ and $A\beta_{42}$ + $PrP_{107–120}$ pre-incubated under conditions promoting ADDL formation prior to addition to the cell medium. All samples were initially in 2% (*v*/*v*) DMSO and F-12 Ham medium at concentrations of 100 and 25 μM (m.e.) for $A\beta_{42}$ and $PrP_{107–120}$, respectively, and were diluted 33-fold before each experiment into cellular medium without DMSO to final concentrations of 3 and 0.75 μM (m.e.) for $A\beta_{42}$ and $PrP_{107–120}$, respectively. Scale bar = 15 μm. **(B)** Semi-quantitative analysis of intracellular Ca^{2+} derived fluorescence. Experimental errors are S.E.M. (n = 4). The triple (***) asterisks refer to p values < 0.001 relative to the untreated cells. The triple (###) symbols refer to p values < 0.001 relative to $A\beta_{42}$ ADDLs.

2.5. $PrP_{107-120}$ Reduces Intracellular Reactive Oxygen Species (ROS) Induced by $A\beta_{42}$ Oligomers

Another effect caused early by $A\beta_{42}$ ADDLs when added to the extracellular medium of cells is the increase of ROS levels in the cytosol [58,61]. We observed an increase of ROS-derived fluorescence up to 190 ± 19% in SH-SY5Y cells treated with $A\beta_{42}$ ADDLs compared with untreated cells, and no significant change in cells treated with $PrP_{107–120}$ alone (Figure 5). By contrast, the treatment with $A\beta_{42}$ ADDLs + $PrP_{107–120}$ and $A\beta_{42}$ + $PrP_{107–120}$ did not cause any significant change in ROS-derived fluorescence levels compared with untreated cells, and levels significantly lower than those observed after treatment with $A\beta_{42}$ ADDLs (Figure 5). Therefore, $PrP_{107–120}$ can effectively protect SH-SY5Y cells against the oxidative stress induced by $A\beta_{42}$ ADDLs.

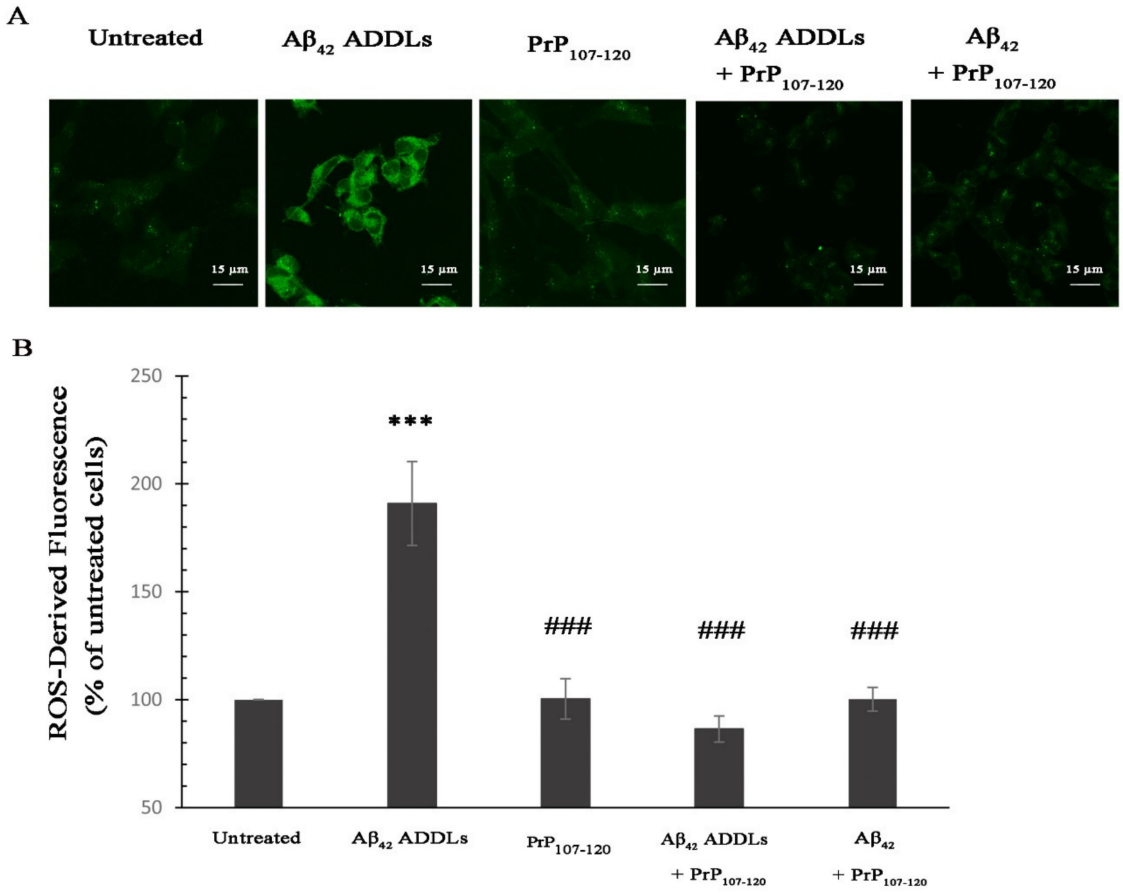

Figure 5. Analysis of intracellular reactive oxygen species (ROS) levels of SH-SY5Y cells treated with $A\beta_{42}$ oligomers and $PrP_{107–120}$. (**A**) Representative scanning confocal microscopy images of intracellular free ROS levels in SH-SY5Y cells loaded with CM-H_2DCFDA. The cells were treated with the same samples described in the Figure 4 legend. Scale bar = 15 µm. (**B**) Semi-quantitative analysis of intracellular ROS-derived fluorescence. Experimental errors are S.E.M. (n = 3). The triple (***) asterisks refer to p values < 0.001 relative to the untreated cells. The triple (###) symbols refer to p values < 0.001 relative to $A\beta_{42}$ ADDLs.

2.6. $PrP_{107-120}$ Reduces the Toxicity of Other Model Oligomers

In order to assess whether the protective role of $PrP_{107–120}$ observed with ADDLs was specific to this peptide and oligomer system or was more generally exerted against misfolded protein oligomers, we also tested whether $PrP_{107–120}$ has the ability to decrease the cytotoxicity of another type of misfolded oligomer, those formed by the model protein HypF-N named type A and found to have effects similar to those of $A\beta_{42}$ [62–65]. We observed an increase of ROS-derived fluorescence in SH-SY5Y cells upon treatment with type A HypF-N oligomers up to 214 ± 39% (Figure 6). Exposure to HypF-N oligomers

+ $PrP_{107–120}$ and HypF-N preincubated with $PrP_{107–120}$ under conditions promoting type A HypF-N oligomer formation showed non-significant changes in intracellular ROS-derived fluorescence (93 ± 2% and 124 ± 19%, respectively).

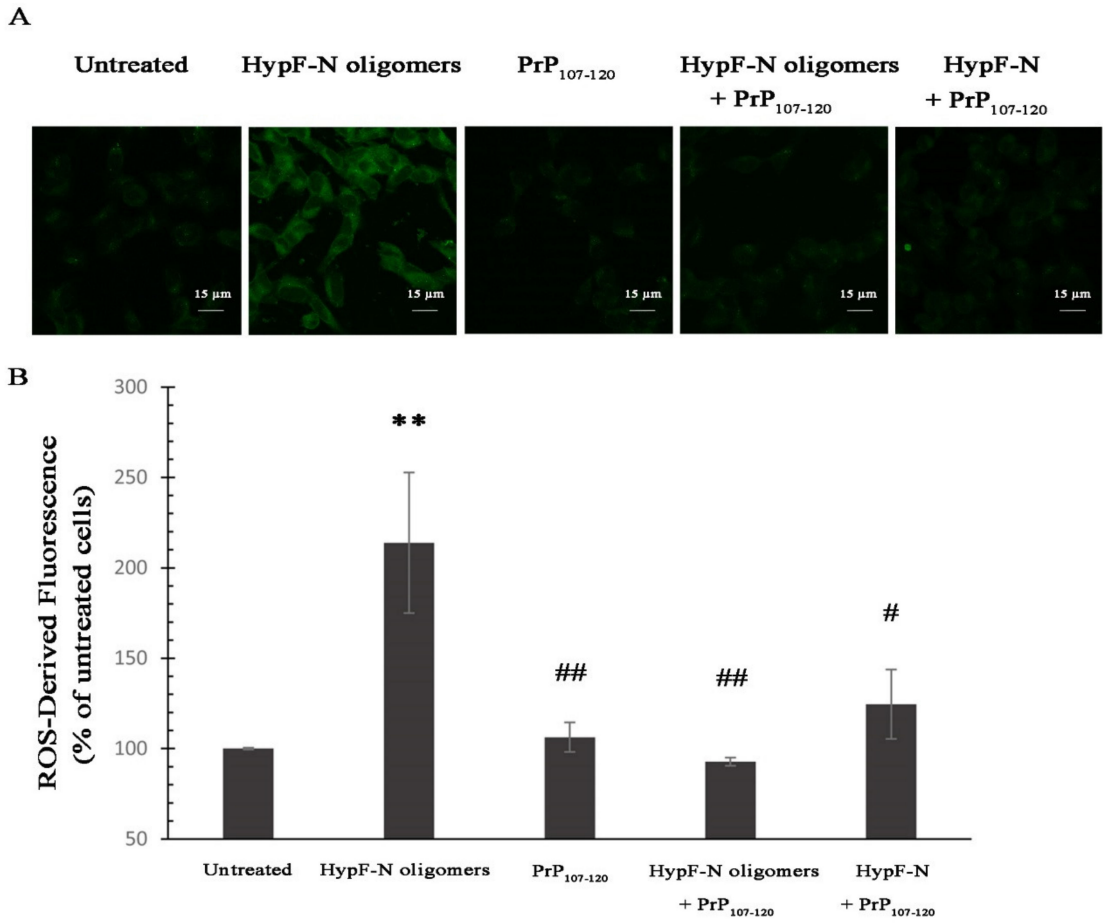

Figure 6. Analysis of intracellular ROS levels of SH-SY5Y cells treated with type A HypF-N oligomers and $PrP_{107–120}$. (**A**) Representative scanning confocal microscopy images of intracellular free ROS levels in SH-SY5Y cells loaded with CM-H_2DCFDA. The cells were treated for 1 h with HypF-N oligomers, $PrP_{107–120}$, HypF-N oligomers + $PrP_{107-120}$ and a sample containing HypF-N and $PrP_{107–120}$ pre-incubated under conditions promoting HypF-N oligomer formation prior to addition to the cell medium. Final HypF-N and $PrP_{107–120}$ concentrations were 12 and 3 µM (m.e.), respectively. Scale bar = 15 µm. (**B**) Semi-quantitative analysis of intracellular ROS-derived fluorescence. Experimental errors are S.E.M. (n = 3). The double (**) asterisks refer to p values < 0.01 relative to the untreated cells. The double (##) and single (#) symbols refer to p values < 0.01 and < 0.05, respectively, relative to HypF-N oligomers.

2.7. $PrP_{107-120}$ Reduces $A\beta_{42}$ ADDLs Internalization in SH-SY5Y Cells

In order to study the effects of $PrP_{107-120}$ on the cellular internalization of $A\beta_{42}$ ADDLs in SH-SY5Y cells, we performed immunostaining experiments using the 6E10 specific antibody against $A\beta_{42}$ and wheat germ agglutinin to stain $A\beta_{42}$ and the cell membrane, respectively. Cells were exposed for 1 h to the various protein samples described above and added to the cell medium. Thus, for the intracellular $A\beta_{42}$-derived fluorescence (green) in the SH-SY5Y cells, we observed more than 78% reduction in cells treated with $A\beta_{42}$ ADDLs + $PrP_{107–120}$, and more than 74% reduction in cells treated with $A\beta_{42}$ + $PrP_{107–120}$ in terms of intracellular ADDLs levels with respect to cells treated with $A\beta_{42}$ ADDLs taken as 100% (Figure 7). These results indicate that $PrP_{107–120}$ is able to significantly reduce $A\beta_{42}$ ADDL internalization in SH-SY5Y cells when added either before or after the $A\beta_{42}$ oligomerization process.

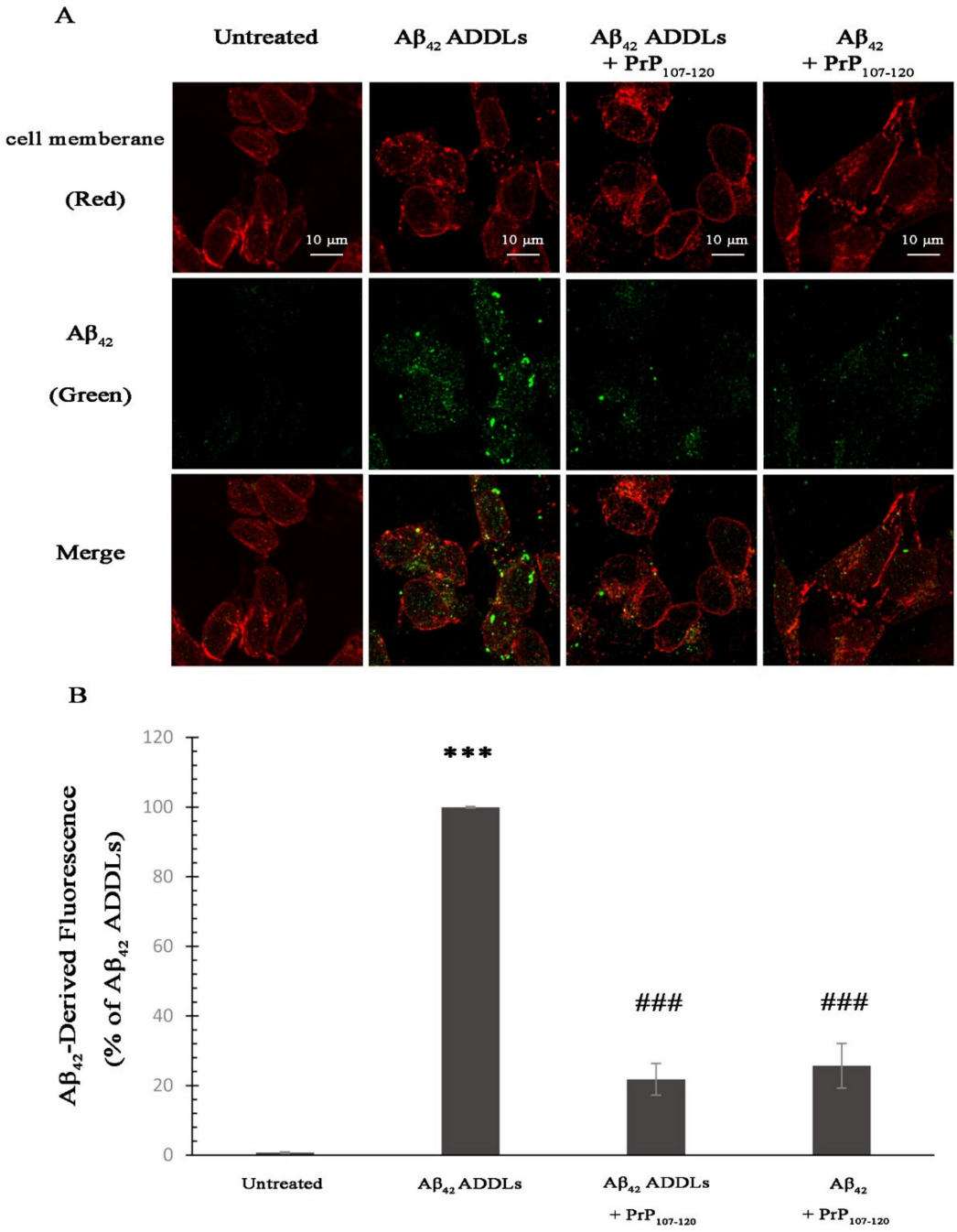

Figure 7. Effect of $PrP_{107–120}$ on $A\beta_{42}$ ADDL internalization in SH-SY5Y cells. (**A**) Representative scanning confocal microscopy images of SH-SY5Y cells treated with the indicated samples and showing $A\beta_{42}$ ADDLs. The cells were treated with the same samples described in the Figure 4 legend. The cellular membrane was stained with wheat germ agglutinin (red fluorescence) and $A\beta_{42}$ ADDLs were labelled with mouse monoclonal primary antibody 6E10 and anti-mouse secondary antibody (green fluorescence). Scale bar = 10 μm. (**B**) Semi-quantitative analysis of intracellular $A\beta_{42}$ ADDL-derived fluorescence. Experimental errors are S.E.M. (n = 3). The triple (***) asterisks refer to p values < 0.001 relative to the untreated cells. The triple (###) symbols refer to p values < 0.001 relative to $A\beta_{42}$ ADDLs.

2.8. $PrP_{107-120}$ Does Not Change the Structure or Aggregation State of $A\beta_{42}$ ADDLs

To determine whether $PrP_{107–120}$ can modify the structure of $A\beta_{42}$ ADDLs into non-toxic $A\beta_{42}$ oligomers or cause a change in their aggregation state (either fibrils, large aggregates or monomers),

we carried out a number of tests using dot-blot, ThT fluorescence, far-UV CD and ANS fluorescence on ADDLs in the presence and absence of $PrP_{107–120}$, using the same samples used for cell toxicity.

The presence of $A\beta_{42}$ ADDLs was monitored by a dot-blot immunoassay using the conformation-sensitive antibody 19.3 specific for $A\beta_{42}$ ADDLs [66] and the monoclonal antibody 6E10, which is able to bind all types of $A\beta_{42}$ species. For $A\beta_{42}$ ADDLs, $A\beta_{42}$ + $PrP_{107–120}$ and $A\beta_{42}$ ADDLs + $PrP_{107–120}$ we observed a recognition for both antibodies, whereas the $PrP_{107–120}$ spot did not show any cross-reaction (Figure 8A), suggesting that $PrP_{107–120}$ cannot change the structure or oligomerization state of ADDLs.

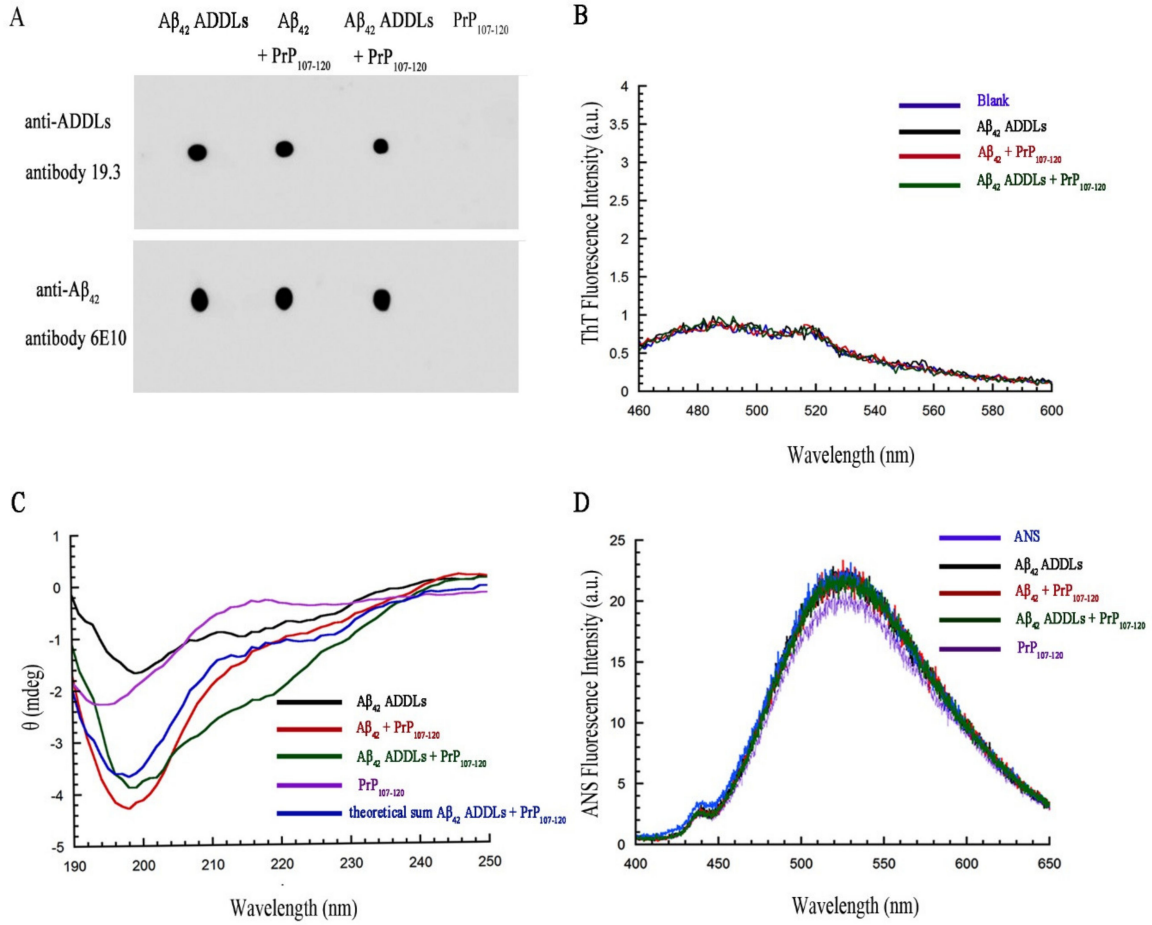

Figure 8. Effect of $PrP_{107–120}$ on $A\beta_{42}$ ADDL structure. (**A**) Dot-blot immunoassay for $A\beta_{42}$ ADDLs, $A\beta_{42}$ + $PrP_{107–120}$, $A\beta_{42}$ ADDLs + $PrP_{107–120}$ and $PrP_{107–120}$ samples. All samples were initially in 2% (*v*/*v*) DMSO and F-12 Ham medium at concentrations of 100 and 25 μM (m.e.) for $A\beta_{42}$ and $PrP_{107–120}$, respectively. They were then spotted in two different nitrocellulose membranes, probed with the conformation-sensitive anti-ADDL antibody 19.3 (first line) and with conformation-insensitive anti-$A\beta_{42}$ antibody 6E10 (second line). (**B**) ThT fluorescence assay for free ThT (blue), $A\beta_{42}$ ADDLs (black), $A\beta_{42}$ + $PrP_{107–120}$ (red) and $A\beta_{42}$ ADDLs + $PrP_{107–120}$ (green). Samples were incubated as described above. ThT assay was carried out at 22 μM ThT (final concentration in the cuvette), pH 6.0, 37 °C. (**C**) Far-UV CD spectra for $A\beta_{42}$ ADDLs (black), $A\beta_{42}$ + $PrP_{107–120}$ (red) and $A\beta_{42}$ ADDLs + $PrP_{107–120}$ (green) and $PrP_{107–120}$ (purple). Samples were incubated as described above and diluted before spectrum acquisition to final concentrations of 22.2 μM $A\beta_{42}$ and 5.55 μM $PrP_{107–120}$, 25 °C. (**D**) ANS fluorescence spectra for free ANS (55 μM final concentration) and the same samples indicated in panel C. Fluorescence spectra were recorded at 25 °C.

$A\beta_{42}$ ADDLs did not bind ThT and did not increase its fluorescence, behavior that was not found to be affected by the $PrP_{107–120}$ peptide (Figure 8B) and suggests that the peptide was not able to change

the structure of the ADDLs into a stable and ThT-positive β-sheet structure. Moreover, the CD spectra observed for the $A\beta_{42}$ + $PrP_{107–120}$ and $A\beta_{42}$ ADDLs + $PrP_{107–120}$ were found to be similar to those resulting from the sum of the spectra of $A\beta_{42}$ ADDLs alone and $PrP_{107–120}$ alone, indicating that the $PrP_{107–120}$ peptide did not significantly change the secondary structure of $A\beta_{42}$ ADDLs (Figure 8C). Finally, the spectrum of ANS in the presence of $A\beta_{42}$ ADDLs did not change if the ADDLs were formed in the presence of the peptide ($A\beta_{42}$ + $PrP_{107–120}$) or pre-incubated in the presence of the peptide after their formation ($A\beta_{42}$ ADDLs + $PrP_{107–120}$), suggesting again that the $PrP_{107–120}$ peptide was not able to change the $A\beta_{42}$ ADDL structure (Figure 8D).

2.9. $PrP_{107-120}$ Does Not Colocalise with $A\beta_{42}$ ADDLs but Partially Colocalises with Cellular PrP^C in SH-SY5Y Cells

The inability of $PrP_{107-120}$ to change the structure of $A\beta_{42}$ ADDLs, yet its ability to decrease ADDL toxicity, raised two possible hypotheses: (i) $PrP_{107-120}$ binds to ADDLs and shields their hydrophobic patches that are responsible for toxicity, or (ii) it interacts with the cells and renders them less vulnerable to ADDL toxicity. To verify which hypothesis was correct, the interaction of $PrP_{107–120}$ and $A\beta_{42}$ was studied in cell cultures. Confocal microscopy images showed an absence of co-localization between $A\beta_{42}$ ADDLs (3 μM m.e.) and $PrP_{107-120}$, both with ratios of 4:1 (0.75 μM $PrP_{107–120}$) and 1:1 (3 μM $PrP_{107–120}$), suggesting an absence of interaction between the two peptides (Figure 9). By contrast, $PrP_{107–120}$ (0.75 μM) was found to partially colocalize with endogenous cellular PrP^C (Figure 10, white arrows). These results also showed a significant, albeit weak, expression of PrP^C in our SH-SY5Y cell system, which is in agreement with the levels of expression of the Human Protein Atlas (Figure 10).

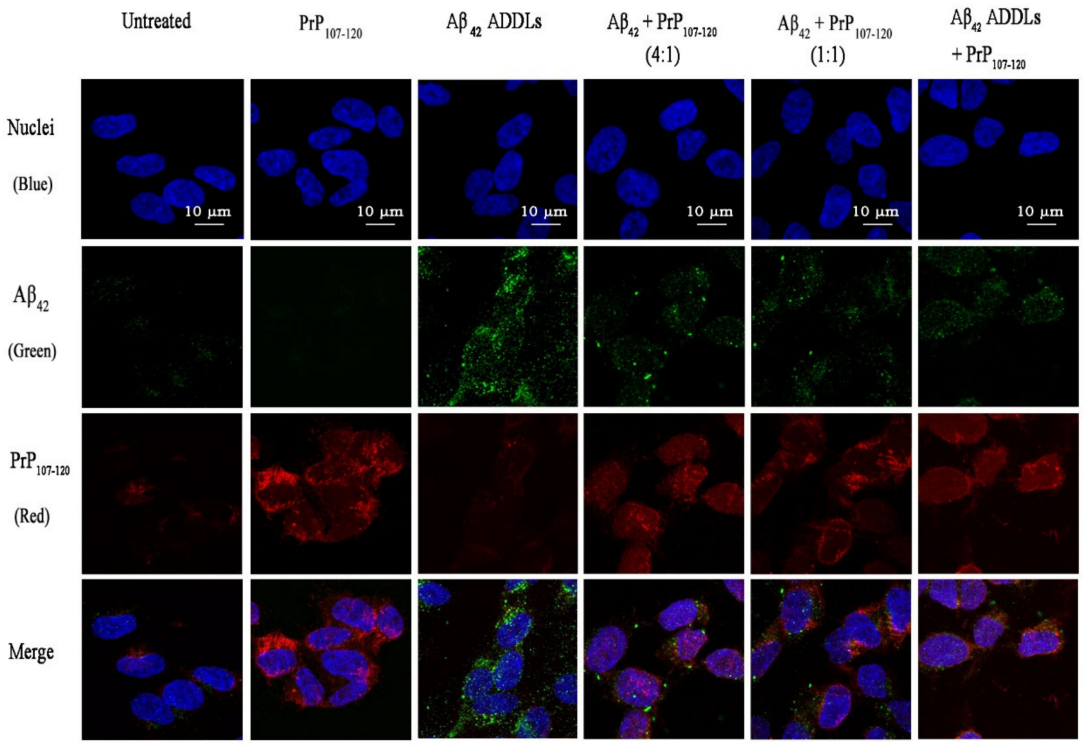

Figure 9. Absence of co-localization of $A\beta_{42}$ ADDLs with $PrP_{107–120}$. Cells were treated for 1 h with the same samples described in the Figure 4 legend and indicated on top of the images (added to the cell medium). $PrP_{107–120}$ was labelled with BODIPY TMR-X NHS Ester (red fluorescence), $A\beta_{42}$ ADDLs with mouse monoclonal primary antibody 6E10 and a secondary antibody (green fluorescence) and the nuclei with the Hoechst dye (blue florescence). Scale bar = 10 μm.

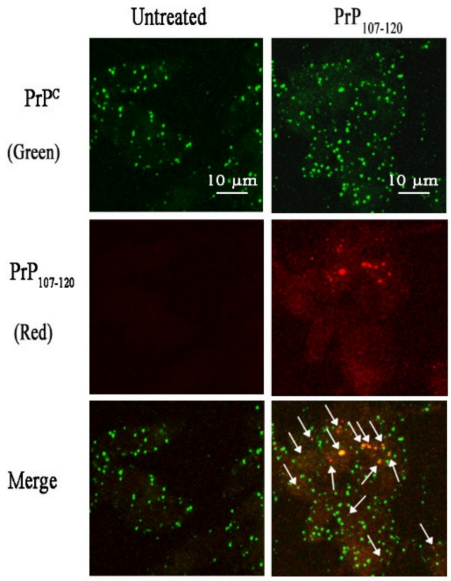

Figure 10. Partial co-localization of $PrP_{107-120}$ with endogenous cellular PrP^C. Cells were treated for 1 h with the $PrP_{107–120}$ sample described in the Figure 9 legend and indicated on top of the images (added to the cell medium). $PrP_{107–120}$ was labelled with BODIPY TMR-X NHS Ester (red fluorescence) and cellular PrP^C was labelled with mouse monoclonal primary antibody PrP (5B2) and Alexa Fluor 488-conjugated anti-mouse secondary (green fluorescence). The white arrows indicate the co-localization spots in the merged images. Scale bar = 10 µm.

3. Discussion

The results obtained here show that the synthetic peptide $PrP_{107–120}$ is soluble and unstructured in solution and can significantly protect neuroblastoma SH-SY5Y cells against a representative form of oligomeric $A\beta_{42}$, namely, ADDLs. In particular, in the presence of the peptide, $A\beta_{42}$ oligomers caused a remarkably lower Ca^{2+} influx from the cellular medium to the cytosol, a remarkably lower increase of cellular ROS and a significantly lower alteration of mitochondrial metabolic activity. Furthermore, they had a remarkably lower ability to enter the cytosol across the cell membrane. The absence of interaction of the $PrP_{107–120}$ peptide with ADDLs, and the partial colocalization of the peptide with endogenous cellular PrP^C, indicates that the peptide protects the cells against $A\beta_{42}$ oligomer toxicity, at least in part, by interfering with cellular PrP^C.

Previous studies have suggested that the cell surface protein PrP^C mediates the toxicity of $A\beta_{42}$ oligomers by binding to them and affecting synaptic plasticity and other neuronal functions [13–18], although a general consensus on this point has not yet been found [19–21]. One PrP^C region of the sequence thought to be involved in $A\beta_{42}$ binding encompasses approximately residues 95–110 [13,14,33–35,37–42]. An antibody raised against residues 93–109 of PrP^C (anti-$PrP^C{}_{93–109}$ GD11) and a synthetic peptide corresponding to residues 98–107 ($PrP_{98–107}$) were found to inhibit the toxicity of the $A\beta_{42}$ ADDLs to organotypic hippocampal slices, whereas a control $PrP_{213–230}$ peptide did not have any such effects [37]. It was proposed that the antibody and the $PrP_{98–107}$ peptide exert their effect by binding to PrP^C and the diffusible $A\beta_{42}$ oligomers, respectively, thus preventing their interaction in both cases [37].

In this study we have used a different perspective: Rather than using a synthetic PrP^C peptide binding to $A\beta_{42}$, we have used a synthetic PrP^C peptide involved in PrP self-recognition ($PrP_{107–120}$), with the goal of achieving a similar biological result with a different mechanism, namely, binding to membrane-anchored PrP^C and impeding the binding of the latter to $A\beta_{42}$ oligomers. We found that $PrP_{107–120}$ significantly reduced the toxicity of $A\beta_{42}$ oligomers with or without pre-incubation of the peptide with $A\beta_{42}$ during the process of ADDL oligomer formation. Biophysical analyses and a dot-blot immunoassay excluded an alteration of the $A\beta_{42}$ ADDL structure or aggregation state in the

presence of the peptide, ruling out the hypothesis that the reduction of $A\beta_{42}$ oligomer toxicity and internalization mediated by $PrP_{107-120}$ is due to this reason. Moreover, no $PrP_{107–120}$ colocalization with $A\beta_{42}$ was found in the cell cultures using confocal microscopy even at high concentrations of $PrP_{107–120}$, indicating a lack of any significant interaction between the two peptide species. In contrast, a partial colocalization between $PrP_{107-120}$ and endogenous PrP^C was found, indicating that the peptide can bind to the cellular prion protein. Furthermore, akin to previous observations, the role of PrP^C in mediating oligomer toxicity is not restricted to $A\beta_{42}$ oligomers, but also to other β-sheet rich proteins [67], and our results indicate a similar effect of $PrP_{107–120}$ on $A\beta_{42}$ oligomers and type-A HypF-N oligomers, used here as a positive control of toxic oligomeric species. However, we cannot completely exclude that $PrP_{107–120}$ stimulates a well-defined intracellular signaling [25] and causes less vulnerability and greater resistance against $A\beta_{42}$ oligomer toxicity independently of its interaction with membrane-anchored PrP^C.

Overall, although the results obtained here in vitro on a cell culture line need to be validated in vivo on animal models, the present study shows the potential therapeutic value of peptides corresponding to the region of the sequence of PrP^C involved in self-recognition, or other molecules potentially mimicking the same sequence trait, for the treatment of AD. This could open new avenues to the identification of the mechanism of interaction of soluble prion-derived peptides and $A\beta_{42}$ oligomers, as well as to the mechanism through which PrP^C mediates the toxic effects of $A\beta_{42}$ oligomers.

4. Materials and Methods

4.1. $PrP_{107–120}$ Preparation

The synthetic human prion protein fragment spanning residues 107–120 ($PrP_{107–120}$) with the sequence Ac-TNMKHMAGAAAAGA (purity by HPLC > 95%) was purchased from Biomatik (Wilmington, DE, USA). The <5% impurities are mainly peptides with similar sequences, as are often found in solid-state peptide synthesis [68]. The counterions of peptide preparations (trifluoroacetate and guanidinium) are not supposed to be cell protectors and did not interfere with our analysis. Metal ions or other agents were not present. The lyophilized peptide was stored at −20 °C, and for each experiment 1 mg of peptide was dissolved in 1 mL of water.

4.2. Preparation of $A\beta_{42}$ ADDLs, $A\beta_{42}$ ADDLs + $PrP_{107–120}$ and $A\beta_{42}$ + $PrP_{107–120}$ Samples

Lyophilized synthetic $A\beta_{42}$ in a trifluoroacetate salt (Bachem, Bubendorf, Switzerland) was dissolved in pure hexafluoro-2-isopropanol (HFIP) to 1 mM. For each experiment, the solvent was evaporated using gentle nitrogen flow and the peptide was reconstituted in 2% (*v*/*v*) dimethyl sulfoxide (DMSO) and F12 Ham medium to a final concentration of 100 μM. Aβ-derived diffusible ligands (ADDLs) were prepared after 24 h incubation at 4 °C, as previously reported [52], and checked for their distinctive characteristics using atomic force microscopy, Western blotting and dot-blot, as previously described [56,57]. In this study, we used the following samples: (A) 100 μM m.e. of $A\beta_{42}$ ADDLs; (B) 25 μM $PrP_{107–120}$ (final concentration) added to preformed 100 μM m.e. of $A\beta_{42}$ ADDLs at a 1:4 molar ratio, incubated at 4 °C for 2 h ($A\beta_{42}$ ADDLs + $PrP_{107–120}$); (C) 25 μM $PrP_{107–120}$ (final concentration) added to 100 μM $A\beta_{42}$ at a 1:4 molar ratio before $A\beta_{42}$ aggregation, maintained at 4 °C for 24 h under the same conditions used to form $A\beta_{42}$ ADDLs ($A\beta_{42}$ + $PrP_{107–120}$); and (D) 25 μM $PrP_{107–120}$. All four samples were in 2% (*v*/*v*) DMSO and F-12 Ham medium and were diluted 33-fold before each experiment into cellular medium without DMSO to final concentrations of 3 and 0.75 μM (m.e.) for $A\beta_{42}$ and $PrP_{107–120}$, respectively.

4.3. Preparation of HypF-N Oligomers

HypF-N was purified as described previously [62] and stored at −80 °C. Before each experiment, the protein sample was thawed, centrifuged at 13,000 rpm (17950× *g*) for 10 min, and the concentration was measured at 280 nm. The sample was then diluted to 48 μM in 12% (*v*/*v*) trifluoroethanol, 50 mM

acetate buffer and 2 mM dithiothreitol, at pH 5.5, as this condition is known to promote aggregation of HypF-N and proteins of the same structural family [62,69]. After 4 h at 25 °C, the sample was centrifuged at 12,000 rpm (15300× *g*) for 15 min and the pellet was dried with a gentle nitrogen flow and resuspended to 12 μM m.e. in cellular medium with or without $PrP_{107–120}$, to a final concentration of 3 μM (4:1 molar ratio).

4.4. Bicinchoninic Acid (BCA) Assay

Stock bovine serum albumin (BSA) standard (Sigma-Aldrich, Saint Louis, MO, USA) was prepared at a 2-mg/mL final concentration in water. Eight BSA samples with concentrations ranging from 0 to 2000 μg/mL were prepared by dilution for the standard curve. The bicinchoninic acid (BCA) working reagent was prepared by mixing 10 mL of solution A (Bicinchoninic Acid solution, Sigma-Aldrich) with 200 μL of solution B (4% *w*/*v* $CuSO_4 \cdot 5H_2O$ in water). The blank and protein samples were mixed with the resulting BCA working reagent at a 1:8 ratio; thus, 25 μL of each peptide or BSA or blank samples were mixed with 200 μL of BCA working reagent and were added to 96-microplate wells. The plate was incubated at 60 °C for 15 min and, after 5 min cooling to room temperature, the absorbance of all wells was measured at 562 nm using an ultrafast BioTek Synergy H1 plate reader (Winooski, VT, USA). All absorbance values were blank subtracted. Peptide concentration was calculated by interpolation using a standard curve (absorbance versus protein concentration) obtained with the eight BSA samples.

4.5. Fibrillation of $PrP_{107–120}$

The aggregation kinetics of $PrP_{107–120}$ was investigated under different solution conditions at 37 °C: (A) 0.5 mg/mL peptide in 20 mM phosphate buffer, 200 mM NaCl, pH 7.0; (B) 0.5 mg/mL peptide in 20 mM HCO_3^-, 200 mM NaCl, pH 10.5; (C) 0.5 mg/mL peptide in 20 mM phosphate buffer, 200 mM NaCl, 10% (*v*/*v*) trifluoroethanol, pH 7.0; (D) 1.0 mg/mL peptide in 20 mM acetate buffer, 200 mM NaCl, pH 4.0; (E) 1.0 mg/mL peptide in 20 mM HCO_3^-, 200 mM NaCl, pH 10.5; (F) 1.0 mg/mL peptide in 20 mM phosphate buffer, 500 mM NaCl, pH 7.0; (G) 1.0 mg/mL peptide in 20 mM phosphate buffer, 15% (*v*/*v*) methanol, pH 7.0; (H) 1.0 mg/mL peptide in 20 mM phosphate buffer, 200 mM Na_2SO_4, pH 7.0. Fibril formation was monitored by the ThT fluorescence assay, DLS and CD spectroscopy for all conditions.

4.6. Dynamic Light Scattering

In a first experiment, to determine the size of monomeric $PrP_{107–120}$, 1 mg of peptide was dissolved in 1 mL of water. The sample was filtered through a 0.22-μm filter and size distribution analysis was performed at 25 °C by a Zetasizer Nano S DLS device from Malvern Panalytical (Malvern, Worcestertshire, UK) thermostated with a Peltier system and checked for its reliability with polystyrene latex beads with known hydrodynamic diameter. A 10-mm plastic cell with a reduced volume was used. The refractive index and viscosity were 1.333 and 0.88 cP. The cell position and attenuator index were set automatically. The theoretical R_h for a peptide was calculated by the following equation:

$$R_h\ (Å) = (2.21 \pm 1.07)\ N^{\,0.57 \pm 0.02} \quad (1)$$

where N is the number of amino acid residues [46]. The theoretical D_h was twice the R_h value. In a second experiment, to investigate the effect of different conditions on peptide aggregation, measurements were carried out using 1 mg of peptide dissolved in 1 mL of selected buffers and following the size distribution over time for several days at 37 °C, using the same technical apparatus and cell described above. The refractive index and viscosity were set according to the various conditions.

4.7. ThT Fluorescence

ThT (Sigma-Aldrich) was dissolved to 25 μM, in 25 mM phosphate buffer, with a pH of 6.0, then filtered by a 0.45-μm filter. For a given peptide sample, 60 μL aliquots were added to 440 μL of resulting

solution. A 2 × 10 mm optical path-length cuvette was used, and fluorescence spectra were recorded at 37 °C using a PerkinElmer LS 55 fluorimeter (Waltham, MA, USA) equipped with a thermostated cell holder attached to a Thermo Haake C25P water bath (Karlsrube, Germany) with an excitation wavelength of 440 nm and an emission wavelength range of 460–600 nm.

4.8. Circular Dichroism (CD) Spectroscopy

To determine the $PrP_{107-120}$ polymerization kinetics in the presence of different conditions, 0.2 mg/mL of $PrP_{107-120}$ peptide was used. To investigate the effect of the $PrP_{107–120}$ peptide on $A\beta_{42}$ oligomeric ADDLs, three samples were prepared, each 300 µL, including two separate samples of 22.2 µM $A\beta_{42}$ ADDLs and one sample containing both 22.2 µM $A\beta_{42}$ and 5.55 µM $PrP_{107–120}$ at a 4:1 molar ratio. For removing DMSO, dialysis was performed using Spectra/Por 3 dialysis kits (MWCO 3.5 kDa, Spectrum Labs/Thermo Fisher Scientific, Waltham, MA, USA) and 10 mM phosphate buffer, with a pH of 6.0, for 3 h at 4 °C. For the preparation of $A\beta_{42}$ ADDLs + $PrP_{107–120}$ sample, $PrP_{107–120}$ was added at a final concentration of 5.55 µM after dialysis and was incubated for 2 h at 4 °C. Far-UV CD spectra were measured at 25 °C between 190–260 nm with a 1-nm spectral step size and 50-nm/min scanning rate on a JASCO J-810 spectropolarimeter (Tokyo, Japan) equipped with thermostated cell-holder attached to a Thermo Haake C25P water bath (Karlsruhe, Germany). A 1-mm thermostated quartz cuvette was used for all CD spectra. Spectra were blank-subtracted and normalized to mean residue ellipticity.

4.9. Cell Culture

Adherent human neuroblastoma SH-SY5Y cells (A.T.C.C, Manassas, VA, USA) were cultured in Dulbecco's Modified Eagle's Medium (DMEM, Sigma-Aldrich), F-12 Ham with 25 mM N-(2-hydroxyethyl)piperazine-N'-(2-ethanesulfonic) acid (HEPES) and $NaHCO_3$, supplemented with 10% fetal bovine serum (FBS), 2 mM glutamine and 1% penicillin/streptomycin and maintained at 37 °C and 5% CO_2. When the cells reached 90% confluence, they were split using 0.25% trypsin-EDTA to a maximum of 20 passages.

4.10. MTT Assay

SH-SY5Y cells were plated at a density of 15×10^3 cells per well in a 96-well plate. After 24 h at 37 °C in a 5% CO_2 atmosphere, cells were incubated for 24 h with different samples ($A\beta_{42}$ ADDLs, $A\beta_{42}$ + $PrP_{107–120}$, $A\beta_{42}$ ADDLs + $PrP_{107–120}$ and $PrP_{107–120}$, all pre-dissolved and pre-incubated in 2% (*v*/*v*) DMSO and F-12 Ham medium, as described above). Final concentrations of $A\beta_{42}$ and $PrP_{107–120}$ in DMEM were 3 and 0.75 µM (m.e.), respectively, with a 4:1 molar ratio. Cells were incubated with 0.5 mg/mL of MTT solution in Roswell Park Memorial Institute (RPMI) medium for 3 h at 37 °C, then with lysis buffer (20% SDS, 50% N,N-dimethylformamide, pH 4.7) for 1 h at 37 °C. The optical density was measured at 590 nm by a microplate reader (BioTek, Winooski, VT, USA).

4.11. Measurement of Intracellular Ca^{2+} Levels

SH-SY5Y cells were seeded on a glass coverslip in a six-well plate at a density of 40×10^3 cells per well. After 24 h, 600 µL of various samples ($A\beta_{42}$ ADDLs, $A\beta_{42}$ + $PrP_{107–120}$, $A\beta_{42}$ ADDLs + $PrP_{107–120}$ and $PrP_{107–120}$, all pre-dissolved and pre-incubated in 2% (*v*/*v*) DMSO and F-12 Ham medium, as described above) were added to cells for 1 h at 37 °C. Final concentrations of $A\beta_{42}$ and $PrP_{107-120}$ in DMEM were 3 and 0.75 µM (m.e.), respectively. After washing with phosphate buffered saline (PBS), cells were loaded with a 4-µM Fluo-4 AM probe (Invitrogen/Thermo Fisher Scientific, Waltham, MA, USA) for 10 min at 37 °C. Imaging was performed after excitation at 488 nm with a TCS SP8 confocal scanning microscopy system (Leica Microsystems, Mannheim, Germany), using a Leica Plan Apo 63x oil immersion objective, taking a series of 1-µm-thick optical sections (1024 × 1024) through the cell depth for each sample and projecting them as a single composite image by superimposition.

A minimum of four images were captured for each sample and four replicates were used for each condition. Images were analyzed using Image J software (NIH, Bethesda, MD, USA).

4.12. Measurement of Intracellular Reactive Oxygen Species (ROS)

To detect intracellular accumulations of ROS, SH-SY5Y cells were cultured for 24 h on glass coverslips in a 6-well plate at a density of 40×10^3 cells per well. The medium was then replaced with 600 µL of various samples ($A\beta_{42}$ ADDLs, $A\beta_{42}$ + $PrP_{107–120}$, $A\beta_{42}$ ADDLs + $PrP_{107–120}$ and $PrP_{107–120}$, all pre-dissolved and pre-incubated in 2% (*v*/*v*) DMSO and F-12 Ham medium, as described above) with final concentrations of 3 and 0.75 µM (m.e.) for $A\beta_{42}$ and $PrP_{107–120}$ in DMEM, respectively. After 45 min, 5 µM of 2,7-dichlorodihydrofluorecein diacetate probe (CM-H2DFDA, Thermo Fisher Scientific, Waltham, MA, USA) was added for 15 min at 37 °C. Finally, cells were washed twice in PBS and then fixed in 2% (*w*/*v*) paraformaldehyde for 10 min at room temperature. Cell image acquisition was performed using the TCS SP8 confocal system described in Section 4.11. All measurements were performed in triplicates and ROS levels were calculated with Image J software (NIH). The ROS detected with this probe included mainly hydrogen peroxide [70].

4.13. Immunofluorescence Staining

SH-SY5Y cells were seeded in glass coverslips for 24 h in a 6-well plate at a density of 40×10^3 cells per well, then exposed to 600 µL of various samples ($A\beta_{42}$ ADDLs, $A\beta_{42}$ + $PrP_{107–120}$, $A\beta_{42}$ ADDLs + $PrP_{107–120}$ and $PrP_{107–120}$, all pre-dissolved and pre-incubated in 2% (*v*/*v*) DMSO and F-12 Ham medium, as described above) with final concentrations of 3 and 0.75 µM (m.e.) for $A\beta_{42}$ and $PrP_{107-120}$ in DMEM, respectively. After 1 h at 37 °C, cells were washed with PBS and stained with 1:1000 diluted Alexa Fluor 633-conjugated wheat germ agglutinin (Life Technologies/Thermo Fisher Scientific, Waltham, MA, USA) for 15 min. Cells were rinsed again and fixed with 2% (*w*/*v*) paraformaldehyde for 10 min at room temperature. After cell membrane permeabilization with 0.5% BSA in PBS + 0.5% Triton X-100, cells were incubated with 1:800 diluted mouse monoclonal 6E10 antibody (BioLegend, San Diego, CA, USA) for 1 h in 37 °C. After washing three times with PBS, cells were incubated with 1:1000 diluted Alexa Fluor 488-conjugated anti-mouse secondary antibody (Life Technologies/Thermo Fisher Scientific, Waltham, MA, USA) for 1 h. All experiments were repeated three times and representative images of confocal microscopy are presented. Fluorescence was quantified with Image J software (NIH).

4.14. Dot Blot

To determine the effect of $PrP_{107–120}$ on ADDLs structure, 2 µL of each sample ($A\beta_{42}$ ADDLs, $A\beta_{42}$ + $PrP_{107–120}$, $A\beta_{42}$ ADDLs + $PrP_{107–120}$ and $PrP_{107–120}$, all dissolved in 2% (*v*/*v*) DMSO and F-12 Ham medium, as described above) were transferred onto a nitrocellulose membrane and allowed to dry for 15 min. For blocking the membrane, 1% (*w*/*v*) BSA in Tris-buffered saline and 0.1% Tween 20 (TBST) was used. After 1 h, the membrane was probed with 1:800 diluted mouse monoclonal antibody 6E10 (BioLegend, San Diego, CA, USA) or with 1:500 human antibody specific to ADDLs (clone 19.3, Creative Biolabs, Shirley, NY, USA) at 4 °C overnight. The day after, the membrane was washed three times and subsequently incubated for 1 h at room temperature with 1:3000 peroxidase-conjugated anti-mouse secondary antibody (Abcam, Cambridge, MA, USA) or 1:1000 peroxidase-conjugated anti-human secondary antibody (EMD Millipore, Temecula, CA, USA). Imaging was performed using an Amersham imager 600 (Cytiva, Washington DC, MD, USA).

4.15. ANS Binding Assay

The ANS solution was prepared by dissolving 30 mg of 8-anilino-1-naphthalenesulfonic acid (ANS, Sigma-Aldrich) in 10 mL of 25-µM phosphate buffer, with a pH of 6.0. After 20 min shaking, the solution was filtered by a 0.45-µm filter. ANS concentration was measured by optical absorbance at 375 nm and diluted in the same buffer to 55 µM. For each experiment, 450 µL of ANS solution was mixed with 50 µL of each sample ($A\beta_{42}$ ADDLs, $A\beta_{42}$ + $PrP_{107–120}$, $A\beta_{42}$ ADDLs + $PrP_{107–120}$ and

$PrP_{107–120}$, all dissolved in 2% (*v*/*v*) DMSO and F-12 Ham medium, as described above) or buffer as a blank. A 2- × 10-mm optical path-length was used and fluorescence spectra were recorded at 25 °C using the same PerkinElmer LS 55 fluorimeter described above, with excitation at 380 nm and emission at 400–650 nm.

4.16. Analysis of ADDLs Co-Localization with $PrP_{107-120}$

BODIPY TMR-X NHS Ester (Thermo Fisher Scientific, Waltham, MA, USA) was dissolved in DMSO. $PrP_{107–120}$ was dissolved in 0.1 M $NaHCO_3$ buffer, with a pH of 7.0. The two solutions were diluted at room temperature with continuous shaking for 1 h in the latter buffer at final concentrations of 3 mM peptide and 0.3 mM dye. Cells were cultured on glass coverslips in a 6-well plate at a density of 40×10^3 cells per well. After 24 h, cells were treated for 1 h with 600 µL of various samples ($A\beta_{42}$ ADDLs, $A\beta_{42}$ + labelled $PrP_{107–120}$, $A\beta_{42}$ ADDLs + labelled $PrP_{107–120}$ and labelled $PrP_{107–120}$, all pre-dissolved and pre-incubated in 2% (*v*/*v*) DMSO and F-12 Ham medium, as described above) with final concentrations of 3 and 0.75 µM (m.e.) for $A\beta_{42}$ and labelled $PrP_{107–120}$ in DMEM, respectively. After rinsing with PBS twice, 1:100 diluted fluorescent dye Hoechest (Immunochemistry Technologies, Bloomington, MN, USA) was added for 10 min at 37 °C. Following four washing steps with PBS, cells were fixed using 2% paraformaldehyde. Permeabilization of cells and $A\beta_{42}$ staining were performed as described above. In another experiment, the concentration of labelled $PrP_{107–120}$ was increased to 100 µM, and a 1:1 ratio for labelled $PrP_{107–120}$ to $A\beta_{42}$ was used in the initial pre-treatment in 2% (*v*/*v*) DMSO and F-12 Ham medium to prepare the $A\beta_{42}$ + labelled $PrP_{107–120}$ sample.

4.17. Analysis of $PrP_{107-120}$ Co-Localization with PrP^C

$PrP_{107-120}$ was labelled with BODIPY TMR-X NHS Ester, as described in Section 4.16. SH-SY5Y cells were cultured on a glass coverslip in a 6-well plate for 24 h at a density of 40×10^3 cells per well. After washing with PBS, cells were treated with 600 µL of labelled peptide at a final concentration of 0.75 µM for 1 h. After washing with PBS twice, 2% paraformaldehyde was added for 10 min. After fixation, cells were incubated with 1:250 diluted mouse monoclonal PrP (5B2) antibody (Santa Cruz Biotechnology, Santa Cruz, CA, USA) for 1 h at 37 °C. After washing with PBS, cells were incubated with 1:1000 diluted Alexa Fluor 488-conjugated anti-mouse secondary antibody (Life Technologies/Thermo Fisher Scientific, Waltham, MA, USA). Imaging was performed after excitation at 488 and 561 nm to detect the cellular prion protein and the $PrP_{107–120}$ peptide, respectively, using the TCS SP8 confocal system described in Section 4.11.

4.18. Statistical Analysis

All data are presented as means ± S.E.M. (standard error of the mean). The difference between groups was analyzed using a Student's t-test. The single (*/#), double (**/##) and triple (***/###) symbols refer to p values < 0.05, < 0.01 and < 0.001, respectively.

Author Contributions: Conceptualization, S.M.H. and F.C.; Data curation, E.R.B. and G.F.; Formal analysis, E.R.B. and G.F.; Funding acquisition, C.C.; Investigation, E.R.B.; Methodology, C.C. and F.C.; Resources, C.C. and F.C.; Supervision, F.C.; Validation, E.R.B.; Visualization, E.R.B. and C.C.; Writing–original draft, E.R.B.; Writing–review & editing, S.M.H., G.F., C.C. and F.C. All authors have read and agreed to the published version of the manuscript.

Funding: This research was founded by Regione Toscana (FAS-Salute 2014, project SUPREMAL) and the Progetto Dipartimento di Eccellenza "Gender Medicine".

Conflicts of Interest: The authors declare no conflict of interest.

Abbreviations

AD	Alzheimer's disease
PrPC	Cellular prion protein
Aβ	Amyloid beta
LTP	Long-term potentiation
GPI	Glycosyl-phosphatidyl-inositol
R_h	Hydrodynamic radius
D_h	Hydrodynamic diameter
ADDLs	Amyloid-derived diffusible ligands
DMSO	Dimethyl sulfoxide
HFIP	Hexafluoro-2-isopropanol
ThT	Thioflavin T
CD	Circular dichroism
DLS	Dynamic light scattering
DMEM	Dulbecco's Modified Eagle's Medium
FBS	Fetal bovine serum
MTT	3-(4,5-dimethylthiazol-2-yl)-2,5-diphenyltetrazolium bromide
ROS	Reactive oxygen species
RPMI	Roswell Park Memorial Institute
BSA	Bovine serum albumin
BCA	Bicinchoninic acid

References

1. Hebert, L.E.; Weuve, J.; Scherr, P.A.; Evans, D.A. Alzheimer disease in the United States (2010–2050) estimated using the 2010 census. *Neurology* **2013**, *80*, 1778–1783. [CrossRef] [PubMed]
2. Bienias, J.L.; Beckett, L.A.; Bennett, D.A.; Wilson, R.S.; Evans, D.A. Design of the Chicago health and aging project (CHAP). *J. Alzheimer's Dis.* **2003**, *5*, 349–355. [CrossRef] [PubMed]
3. Kelley, B.J.; Petersen, R.C. Alzheimer's disease and mild cognitive impairment. *Neurol. Clin.* **2007**, *25*, 577–609. [CrossRef] [PubMed]
4. Goedert, M. Tau protein and the neurofibrillary pathology of Alzheimer's disease. *Trends Neurosci.* **1993**, *16*, 460–465. [CrossRef]
5. Huang, H.C.; Jiang, Z.F. Accumulated amyloid-β peptide and hyperphosphorylated tau protein: Relationship and links in Alzheimer's disease. *J. Alzheimer's Dis.* **2009**, *16*, 15–27. [CrossRef] [PubMed]
6. Benilova, I.; Karran, E.; De Strooper, B. The toxic Aβ oligomer and Alzheimer's disease: An emperor in need of clothes. *Nat. Neurosci.* **2012**, *15*, 349. [CrossRef]
7. Selkoe, D.J.; Hardy, J. The amyloid hypothesis of Alzheimer's disease at 25 years. *EMBO Mol. Med.* **2016**, *8*, 595–608. [CrossRef]
8. Hu, N.W.; Smith, I.M.; Walsh, D.M.; Rowan, M.J. Soluble amyloid-β peptides potently disrupt hippocampal synaptic plasticity in the absence of cerebrovascular dysfunction in vivo. *Brain* **2008**, *131*, 2414–2424. [CrossRef]
9. Li, S.; Jin, M.; Koeglsperger, T.; Shepardson, N.E.; Shankar, G.M.; Selkoe, D.J. Soluble Aβ oligomers inhibit long-term potentiation through a mechanism involving excessive activation of extrasynaptic NR2B-containing NMDA receptors. *J. Neurosci.* **2011**, *31*, 6627–6638. [CrossRef]
10. Fischer, B.; Schmoll, H.; Platt, D.; Popa-Wagner, A.; Riederer, P.; Bauer, J. Complement C1q and C3 mRNA expression in the frontal cortex of Alzheimer's patients. *J. Mol. Med.* **1995**, *73*, 465–471. [CrossRef]
11. Yasojima, K.; Schwab, C.; McGeer, E.G.; McGeer, P.L. Up-regulated production and activation of the complement system in Alzheimer's disease brain. *Am. J. Pathol.* **1999**, *154*, 927–936. [CrossRef]
12. Larson, M.E.; Lesné, S.E. Soluble Aβ oligomer production and toxicity. *J. Neurochem.* **2012**, *120*, 125–139. [CrossRef] [PubMed]
13. Barry, A.E.; Klyubin, I.; Mc Donald, J.M.; Mably, A.J.; Farrell, M.A.; Scott, M.; Walsh, D.M.; Rowan, M.J. Alzheimer's disease brain-derived amyloid-β-mediated inhibition of LTP in vivo is prevented by immunotargeting cellular prion protein. *J. Neurosci.* **2011**, *31*, 7259–7263. [CrossRef] [PubMed]

14. Freir, D.B.; Nicoll, A.J.; Klyubin, I.; Panico, S.; Mc Donald, J.M.; Risse, E.; Asante, E.A.; Farrow, M.A.; Sessions, R.B.; Saibil, H.R.; et al. Interaction between prion protein and toxic amyloid β assemblies can be therapeutically targeted at multiple sites. *Nat. Commun.* **2011**, 2336. [CrossRef]
15. Klyubin, I.; Nicoll, A.J.; Khalili-Shirazi, A.; Farmer, M.; Canning, S.; Mably, A.; Linehan, J.; Brown, A.; Wakeling, M.; Brandner, S.; et al. Peripheral administration of a humanized anti-PrP antibody blocks Alzheimer's disease Aβ synaptotoxicity. *J. Neurosci.* **2014**, *34*, 6140–6145. [CrossRef]
16. Um, J.W.; Strittmatter, S.M. Amyloid-β induced signaling by cellular prion protein and Fyn kinase in Alzheimer disease. *Prion* **2013**, *7*, 37–41. [CrossRef]
17. Gimbel, D.A.; Nygaard, H.B.; Coffey, E.E.; Gunther, E.C.; Laurén, J.; Gimbel, Z.A.; Strittmatter, S.M. Memory impairment in transgenic Alzheimer mice requires cellular prion protein. *J. Neurosci.* **2010**, *30*, 6367–6374. [CrossRef]
18. Younan, N.D.; Chen, K.F.; Rose, R.S.; Crowther, D.C.; Viles, J.H. Prion protein stabilizes amyloid-β (Aβ) oligomers and enhances Aβ neurotoxicity in a Drosophila model of Alzheimer's disease. *J. Biol. Chem.* **2018**, *293*, 13090–13099. [CrossRef]
19. Balducci, C.; Beeg, M.; Stravalaci, M.; Bastone, A.; Sclip, A.; Biasini, E.; Tapella, L.; Colombo, L.; Manzoni, C.; Borsello, T.; et al. Synthetic amyloid-β oligomers impair long-term memory independently of cellular prion protein. *Proc. Natl. Acad. Sci. USA* **2010**, *107*, 2295–2300. [CrossRef]
20. Calella, A.M.; Farinelli, M.; Nuvolone, M.; Mirante, O.; Moos, R.; Falsig, J.; Mansuy, I.M.; Aguzzi, A. Prion protein and Aβ-related synaptic toxicity impairment. *EMBO Mol. Med.* **2010**, *2*, 306–314. [CrossRef]
21. Kessels, H.W.; Nguyen, L.N.; Nabavi, S.; Malinow, R. The prion protein as a receptor for amyloid-β. *Nature* **2010**, *466*, E3–E4. [CrossRef]
22. Li, S.; Selkoe, D.J. A mechanistic hypothesis for the impairment of synaptic plasticity by soluble Aβ oligomers from Alzheimer's brain. *J. Neurochem.* **2020**. [CrossRef] [PubMed]
23. Bruce, M.E.; McBride, P.A.; Farquhar, C.F. Precise targeting of the pathology of the sialoglycoprotein, PrP, and vacuolar degeneration in mouse scrapie. *Neurosci. Lett.* **1989**, *102*, 1–6. [CrossRef]
24. Roucou, X.; Gains, M.; LeBlanc, A.C. Neuroprotective functions of prion protein. *J. Neurosci. Res.* **2004**, *75*, 153–161. [CrossRef]
25. Westergard, L.; Christensen, H.M.; Harris, D.A. The cellular prion protein (PrPC): Its physiological function and role in disease. *Biochim. Biophys. Acta (BBA)-Mol. Basis Dis.* **2007**, *1772*, 629–644. [CrossRef]
26. Zahn, R.; Liu, A.; Lührs, T.; Riek, R.; von Schroetter, C.; García, F.L.; Billeter, M.; Calzolai, L.; Wider, G.; Wüthrich, K. NMR solution structure of the human prion protein. *Proc. Natl. Acad. Sci. USA* **2000**, *97*, 145–150. [CrossRef] [PubMed]
27. Zuegg, J.; Gready, J.E. Molecular dynamics simulation of human prion protein including both N-linked oligosaccharides and the GPI anchor. *Glycobiology* **2000**, *10*, 959–974. [CrossRef] [PubMed]
28. Acevedo-Morantes, C.Y.; Wille, H. The structure of human prions: From biology to structural models—Considerations and pitfalls. *Viruses* **2014**, *6*, 3875–3892. [CrossRef]
29. Zomosa-Signoret, V.; Arnaud, J.D.; Fontes, P.; Alvarez-Martinez, M.T.; Liautard, J.P. Physiological role of the cellular prion protein. *Vet. Res.* **2008**, *39*, 1–16. [CrossRef]
30. Pan, K.M.; Baldwin, M.; Nguyen, J.; Gasset, M.; Serban, A.N.A.; Groth, D.; Mehlhorn, I.; Huang, Z.; Fletterick, R.J.; Cohen, F.E. Conversion of alpha-helices into beta-sheets features in the formation of the scrapie prion proteins. *Proc. Natl. Acad. Sci. USA* **1990**, *90*, 10962–10966. [CrossRef]
31. Prusiner, S.B. Prions. *Proc. Natl. Acad. Sci. USA* **1998**, *95*, 13363–13383. [CrossRef] [PubMed]
32. Collinge, J. Prion diseases of humans and animals: Their causes and molecular basis. *Annu. Rev. Neurosci.* **2001**, *24*, 519–550. [CrossRef] [PubMed]
33. Purro, S.A.; Nicoll, A.J.; Collinge, J. Prion protein as a toxic acceptor of amyloid-β oligomers. *Biol. Psychiatry* **2018**, *83*, 358–368. [CrossRef] [PubMed]
34. Zhang, Y.; Zhao, Y.; Zhang, L.; Yu, W.; Wang, Y.; Chang, W. Cellular prion protein as a receptor of toxic amyloid-β42 oligomers is important for Alzheimer's disease. *Front. Cell. Neurosci.* **2019**, *13*, 339. [CrossRef] [PubMed]
35. Laurén, J.; Gimbel, D.A.; Nygaard, H.B.; Gilbert, J.W.; Strittmatter, S.M. Cellular prion protein mediates impairment of synaptic plasticity by amyloid-β oligomers. *Nature* **2009**, *457*, 1128–1132. [CrossRef] [PubMed]
36. Chen, S.; Yadav, S.P.; Surewicz, W.K. Interaction between human prion protein and Amyloid-β (Aβ) oligomers role of N-terminal residues. *J. Biol. Chem.* **2010**, *285*, 26377–26383. [CrossRef] [PubMed]

37. Kudo, W.; Lee, H.P.; Zou, W.Q.; Wang, X.; Perry, G.; Zhu, X.; Smith, M.A.; Petersen, R.B.; Lee, H.G. Cellular prion protein is essential for oligomeric amyloid-β-induced neuronal cell death. *Hum. Mol. Genet.* **2012**, *21*, 1138–1144. [CrossRef]
38. Larson, M.; Sherman, M.A.; Amar, F.; Nuvolone, M.; Schneider, J.A.; Bennett, D.A.; Aguzzi, A.; Lesné, S.E. The complex PrPc-Fyn couples human oligomeric Aβ with pathological Tau changes in Alzheimer's disease. *J. Neurosci.* **2012**, *32*, 16857–16871. [CrossRef]
39. Cox, T.O.; Gunther, E.C.; Brody, A.H.; Chiasseu, M.T.; Stoner, A.; Smith, L.M.; Haas, L.T.; Hammersley, J.; Rees, G.; Dosanjh, B.; et al. Anti-PrPC antibody rescues cognition and synapses in transgenic alzheimer mice. *Ann. Clin. Transl. Neurol.* **2019**, *6*, 554–574. [CrossRef]
40. Fluharty, B.R.; Biasini, E.; Stravalaci, M.; Sclip, A.; Diomede, L.; Balducci, C.; La Vitola, P.; Messa, M.; Colombo, L.; Forloni, G.; et al. An N-terminal fragment of the prion protein binds to amyloid-β oligomers and inhibits their neurotoxicity in vivo. *J. Biol. Chem.* **2013**, *288*, 7857–7866. [CrossRef]
41. Dohler, F.; Sepulveda-Falla, D.; Krasemann, S.; Altmeppen, H.; Schlüter, H.; Hildebrand, D.; Zerr, I.; Matschke, J.; Glatzel, M. High molecular mass assemblies of amyloid-β oligomers bind prion protein in patients with Alzheimer's disease. *Brain* **2014**, *137*, 873–886. [CrossRef] [PubMed]
42. Kostylev, M.A.; Kaufman, A.C.; Nygaard, H.B.; Patel, P.; Haas, L.T.; Gunther, E.C.; Vortmeyer, A.; Strittmatter, S.M. Prion-protein-interacting amyloid-β oligomers of high molecular weight are tightly correlated with memory impairment in multiple Alzheimer mouse models. *J. Biol. Chem.* **2015**, *290*, 17415–17438. [CrossRef] [PubMed]
43. Gu, Y.; Fujioka, H.; Mishra, R.S.; Li, R.; Singh, N. Prion peptide 106–126 modulates the aggregation of cellular prion protein and induces the synthesis of potentially neurotoxic transmembrane PrP. *J. Biol. Chem.* **2002**, *277*, 2275–2286. [CrossRef] [PubMed]
44. Kuwata, K.; Matumoto, T.; Cheng, H.; Nagayama, K.; James, T.L.; Roder, H. NMR-detected hydrogen exchange and molecular dynamics simulations provide structural insight into fibril formation of prion protein fragment 106–126. *Proc. Natl. Acad. Sci. USA* **2003**, *100*, 14790–14795. [CrossRef] [PubMed]
45. Norstrom, E.M.; Mastrianni, J.A. The AGAAAAGA palindrome in PrP is required to generate a productive PrPSc-PrPC complex that leads to prion propagation. *J. Biol. Chem.* **2005**, *280*, 27236–27243. [CrossRef] [PubMed]
46. Bergström, A.L.; Chabry, J.; Bastholm, L.; Heegaard, P.M. Oxidation reduces the fibrillation but not the neurotoxicity of the prion peptide PrP106–126. *Biochim. Biophys. Acta (BBA)-Proteins Proteom.* **2007**, *1774*, 1118–1127.
47. Walsh, P.; Simonetti, K.; Sharpe, S. Core structure of amyloid fibrils formed by residues 106–126 of the human prion protein. *Structure* **2009**, *17*, 417–426. [CrossRef]
48. Walsh, P.; Neudecker, P.; Sharpe, S. Structural Properties and Dynamic Behavior of Nonfibrillar Oligomers Formed by PrP (106−126). *J. Am. Chem. Soc.* **2010**, *132*, 7684–7695. [CrossRef]
49. Sengupta, I.; Udgaonkar, J.B. Structural mechanisms of oligomer and amyloid fibril formation by the prion protein. *Chem. Commun.* **2018**, *54*, 6230–6242. [CrossRef]
50. Florio, T.; Paludi, D.; Villa, V.; Principe, D.R.; Corsaro, A.; Millo, E.; Damonte, G.; D'arrigo, C.; Russo, C.; Schettini, G.; et al. Contribution of two conserved glycine residues to fibrillogenesis of the 106–126 prion protein fragment. Evidence that a soluble variant of the 106–126 peptide is neurotoxic. *J. Neurochem.* **2003**, *85*, 62–72. [CrossRef]
51. Wilkins, D.K.; Grimshaw, S.B.; Receveur, V.; Dobson, C.M.; Jones, J.A.; Smith, L.J. Hydrodynamic radii of native and denatured proteins measured by pulse field gradient NMR techniques. *Biochemistry* **1999**, *38*, 16424–16431. [CrossRef] [PubMed]
52. Lambert, M.P.; Viola, K.L.; Chromy, B.A.; Chang, L.; Morgan, T.E.; Yu, J.; Venton, D.L.; Krafft, G.A.; Finch, C.E.; Klein, W.L. Vaccination with soluble Aβ oligomers generates toxicity-neutralizing antibodies. *J. Neurochem.* **2001**, *79*, 595–605. [CrossRef] [PubMed]
53. Cascella, R.; Evangelisti, E.; Bigi, A.; Becatti, M.; Fiorillo, C.; Stefani, M.; Chiti, F.; Cecchi, C. Soluble oligomers require a ganglioside to trigger neuronal calcium overload. *J. Alzheimer's Dis.* **2017**, *60*, 923–938. [CrossRef]
54. Gong, Y.; Chang, L.; Viola, K.L.; Lacor, P.N.; Lambert, M.P.; Finch, C.E.; Krafft, G.A.; Klein, W.L. Alzheimer's disease-affected brain: Presence of oligomeric Aβ ligands (ADDLs) suggests a molecular basis for reversible memory loss. *Proc. Natl. Acad. Sci. USA* **2003**, *100*, 10417–10422.

55. Ghadami, S.A.; Chia, S.; Ruggeri, F.S.; Meisl, G.; Bemporad, F.; Habchi, J.; Cascella, R.; Dobson, C.M.; Vendruscolo, M.; Knowles, T.P.; et al. Transthyretin inhibits primary and secondary nucleations of amyloid-β peptide aggregation and reduces the toxicity of its oligomers. *Biomacromolecules* **2020**, *21*, 1112–1125. [CrossRef]
56. Limbocker, R.; Chia, S.; Ruggeri, F.S.; Perni, M.; Cascella, R.; Heller, G.T.; Meisl, G.; Mannini, B.; Habchi, J.; Michaels, T.C.; et al. Trodusquemine enhances Aβ 42 aggregation but suppresses its toxicity by displacing oligomers from cell membranes. *Nat. Commun.* **2019**, *10*, 1–13. [CrossRef] [PubMed]
57. Banchelli, M.; Cascella, R.; D'Andrea, C.; Cabaj, L.; Osticioli, I.; Ciofini, D.; Li, M.S.; Skupień, K.; de Angelis, M.; Siano, S.; et al. Nanoscopic insights into the surface conformation of neurotoxic amyloid β oligomers. *RSC Adv.* **2020**, *10*, 21907–21913. [CrossRef]
58. De Felice, F.G.; Velasco, P.T.; Lambert, M.P.; Viola, K.; Fernandez, S.J.; Ferreira, S.T.; Klein, W.L. Aβ oligomers induce neuronal oxidative stress through an N-methyl-D-aspartate receptor-dependent mechanism that is blocked by the Alzheimer drug memantine. *J. Biol. Chem.* **2007**, *282*, 11590–11601. [CrossRef]
59. Lacor, P.N.; Buniel, M.C.; Furlow, P.W.; Clemente, A.S.; Velasco, P.T.; Wood, M.; Viola, K.L.; Klein, W.L. Aβ oligomer-induced aberrations in synapse composition, shape, and density provide a molecular basis for loss of connectivity in Alzheimer's disease. *J. Neurosci.* **2007**, *27*, 796–807. [CrossRef]
60. Demuro, A.; Mina, E.; Kayed, R.; Milton, S.C.; Parker, I.; Glabe, C.G. Calcium dysregulation and membrane disruption as a ubiquitous neurotoxic mechanism of soluble amyloid oligomers. *J. Biol. Chem.* **2005**, *280*, 17294–17300. [CrossRef]
61. Cenini, G.; Cecchi, C.; Pensalfini, A.; Bonini, S.A.; Ferrari-Toninelli, G.; Liguri, G.; Memo, M.; Uberti, D. Generation of reactive oxygen species by beta amyloid fibrils and oligomers involves different intra/extracellular pathways. *Amino Acids* **2010**, *38*, 1101–1106. [CrossRef]
62. Campioni, S.; Mannini, B.; Zampagni, M.; Pensalfini, A.; Parrini, C.; Evangelisti, E.; Relini, A.; Stefani, M.; Dobson, C.M.; Cecchi, C.; et al. A causative link between the structure of aberrant protein oligomers and their toxicity. *Nat. Chem. Biol.* **2010**, *6*, 140–147. [CrossRef]
63. Zampagni, M.; Cascella, R.; Casamenti, F.; Grossi, C.; Evangelisti, E.; Wright, D.; Becatti, M.; Liguri, G.; Mannini, B.; Campioni, S.; et al. A comparison of the biochemical modifications caused by toxic and non-toxic protein oligomers in cells. *J. Cell. Mol. Med.* **2011**, *15*, 2106–2116. [CrossRef] [PubMed]
64. Evangelisti, E.; Cecchi, C.; Cascella, R.; Sgromo, C.; Becatti, M.; Dobson, C.M.; Chiti, F.; Stefani, M. Membrane lipid composition and its physicochemical properties define cell vulnerability to aberrant protein oligomers. *J. Cell Sci.* **2012**, *125*, 2416–2427. [CrossRef] [PubMed]
65. Cascella, R.; Conti, S.; Tatini, F.; Evangelisti, E.; Scartabelli, T.; Casamenti, F.; Wilson, M.R.; Chiti, F.; Cecchi, C. Extracellular chaperones prevent Aβ42-induced toxicity in rat brains. *Biochim. Biophys. Acta (BBA)-Mol. Basis Dis.* **2013**, *1832*, 1217–1226. [CrossRef] [PubMed]
66. Savage, M.; Shughrue, P.; Wolfe, A.; McCampbell, A. Method for Detection of Amyloid Beta Oligomers in a Fluid Sample and Uses Thereof. U.S. Patent Application No. 13/544,554, 28 2013.
67. Resenberger, U.K.; Harmeier, A.; Woerner, A.C.; Goodman, J.L.; Müller, V.; Krishnan, R.; Vabulas, R.M.; Kretzschmar, H.A.; Lindquist, S.; Hartl, F.U.; et al. The cellular prion protein mediates neurotoxic signalling of β-sheet-rich conformers independent of prion replication. *EMBO J.* **2011**, *30*, 2057–2070. [CrossRef]
68. Picotti, P.; De Franceschi, G.; Frare, E.; Spolaore, B.; Zambonin, M.; Chiti, F.; de Laureto, P.P.; Fontana, A. Amyloid fibril formation and disaggregation of fragment 1-29 of apomyoglobin: Insights into the effect of pH on protein fibrillogenesis. *J. Mol. Biol.* **2007**, *367*, 1237–1245. [CrossRef]
69. De Simone, A.; Dhulesia, A.; Soldi, G.; Vendruscolo, M.; Hsu, S.T.D.; Chiti, F.; Dobson, C.M. Experimental free energy surfaces reveal the mechanisms of maintenance of protein solubility. *Proc. Natl. Acad. Sci. USA* **2011**, *108*, 21057–21062. [CrossRef]
70. Yang, C.; Jiang, L.; Zhang, H.; Shimoda, L.A.; DeBerardinis, R.J.; Semenza, G.L. Analysis of hypoxia-induced metabolic reprogramming. In *Methods in Enzymology*; Academic Press: Cambridge, MA, USA, 2014; Volume 542, pp. 425–455.